5-2017

A study of the photoacoustic effect in ethylene gas

Jay Nguyen
University of Tennessee at Chattanooga, kgy362@mocs.utc.edu

A Study of the Photoacoustic Effect in Ethylene Gas

Jay Thanh Nguyen

Departmental Honors Thesis
The University of Tennessee at Chattanooga
Department of Chemistry and Physics

Examination Date: 27 March 2017

Dr. Han J. Park, Ph.D.
Assistant Professor of Chemistry and Associate Department Head
Thesis Director

Dr. Manuel F. Santiago, Ph.D.
Benjamin H. Gross Professor and Department Head
Department Examiner

Dr. Titus V. Albu, Ph.D.
Associate Professor of Chemistry
Department Examiner

Dedication

To my mentor,

whose passion for learning

has inspired

many of

my own

academic endeavors.

And to my parents,

Thanh and Chung Nguyen.

Table of Contents

List of Figures

List of Tables

List of Equations

List of Variables

- Acoustic pressure amplitude, p_0 (in $N \bullet m^{-2}$)
- Optical absorption coefficient, γ (in m^{-1})
- Power of the light source, P (in W)
- Resonance frequency, f_{res} (in Hz)
- Speed of sound, C_s (in cm/s)
- Internal length of the cavity resonator, L (in cm)
- Gas constant, R (in units)
- Temperature, T (in K)
- Relative concentration of the analyte-buffer gas contained within the cavity resonator expressed as the theoretical molecular mass of the analyte-buffer gas, M (in g/mol)
- Percent transmittance, %T
- Power of the radiation that reached the thermal power sensor without initial transmittance through the window, P_i (in W)
- Power of the radiation that reached the thermal power sensor with initial transmittance through the window, P_f

List of Abbreviations

- ACC: 1-aminocyclopropane-1-carboxylic acid
- ARDS: acute respiratory distress syndrome
- C_2H_4: ethylene
- CAS: Chemical Abstracts Service
- CO_x: carbon oxide
- FT-IR: Fourier transform infrared spectroscopy
- GC: gas chromatography
- Ge: germanium
- He: helium
- ICP: integrated circuit piezoelectric
- IR: infrared
- Ne: neon
- NH_4^+: ammonium
- NO_3^-: nitrate
- NO_x: nitrogen oxide
- O_3: ozone
- PA: photoacoustic
- SAM: S-adenosyl-L-methionine
- SF_6: sulfur hexafluoride
- SO_x: sulfur oxide
- UTC: University of Tennessee at Chattanooga
- UV: ultraviolet

Abstract

A Study of the Photoacoustic Effect in Ethylene Gas

By: Jay Nguyen

Ethylene, C_2H_4, is a plant hormone produced and released naturally by plants and soil microorganisms. This colorless, flammable gas has a slightly sweet odor usually only recognized by those who have handled ethylene before. *In situ* analyses of this gas and many other potentially harmful gases outside of the laboratory are often difficult to perform due to the lack of a portable yet reliable unit capable of precisely and accurately detecting and measuring the concentrations of these gases at trace gas concentrations of a few parts per billion. In this research project, photoacoustic spectroscopy was used to detect and measure the concentration of ethylene. Multiple aspects of the experimental setup were independently manipulated to determine each of their effects on the photoacoustic behavior exhibited. The data obtained in this research project was used to help formulate a discussion about what experimental conditions were most ideal for detection and measurement of ethylene using photoacoustic spectroscopy. It was determined that this technique was most reliable when the internal radius of the cavity resonator was small, the power of the light source was high, the concentration of ethylene gas was high, and the rotational frequency of the mechanical chopper was low. These experimental conditions should be considered by manufacturers when devising highly-sensitive, low-cost portable systems for the detection and measurement of ethylene gas both inside and outside the laboratory.

Chapter 1: Introduction

Table of Contents

1.1: Importance of trace gas detection

The idea that unregulated levels of gases can pose adverse health effects on humans and other living organisms is well supported. There exist numerous arguments supporting the need for advanced trace gas detection and analysis techniques. Such claims are often driven by those heavily invested in environmental, microbiological, and/or medical research (1, 2).

Among the many applications of environmental research include targeted studies involving the chemical makeup of the atmosphere, particularly within the troposphere. Such atmospheric chemicals include sulfur oxides, SO_x, nitrogen oxides, NO_x, carbon oxides, CO_x, and various other

pollutants and greenhouse gases (1). Perhaps one of the most well-known but not necessarily well-understood chemicals is ozone, O_3. Ozone is commonly used to sterilize medical tools, to treat water, and to help preserve food. The creation of a hole around the stratosphere and troposphere and the subsequent increase in solar ultraviolet (UV) radiation into the Earth's atmosphere due to the partial destruction of the ozone layer has generated global concern among scientists and nonscientists over the years. At low concentrations, ozone exposure has been linked to respiratory problems, skin rashes, and irritation to the eyes. Therefore, the ability to reliably detect and measure the concentration of chemicals in the environment at any level is of paramount importance (3). Within the field of microbiology, trace gas detection and analysis techniques such gas chromatography together with flame ionization detection and gas chromatography together with photon ionization detection are utilized to better understand the occurrence of nitrogen fixation in nature. Many biological systems cannot metabolize molecular nitrogen; they must first convert, or fix, diatomic nitrogen into some other usable form such as ammonium ion, NH_4^+, or nitrate ion, NO_3^-. The nitrogen fixation process can be better understood by observing the production of either of these two nitrogenous compounds. A medical application of trace gas detection involves the physical and chemical analyses of exhaled air to help diagnosis some common conditions. Gases produced via the body's natural metabolic processes can accumulate within the lungs before being exhaled. Exhaled air with a sweet odor can indicate uncontrolled diabetes, a fishy odor can indicate advanced liver disease, and an urine-like odor can indicate kidney failure (2).

There exist numerous other practical applications supporting the need for advanced trace gas detection techniques. Another practical application of trace gas detection involves the

combined use of physical chemistry and analytical chemistry to detect and measure the concentration of the chemical ethylene.

1.2: Importance of trace ethylene detection

Ethylene, C_2H_4, is a phytohormone, or plant hormone, produced and released naturally by plants and soil microorganisms (4, 5). This plant hormone is actively involved in almost all stages of plant development. Seed growth and germination, leaf growth, and leaf and fruit abscission are among the many plant processes regulated by ethylene (6). For climacteric fruits, or fruits that continue to ripen after being harvested, the presence of ethylene further encourages ripening. For non-climacteric fruits, or fruits that do not continue to ripen after being harvested, the presence of ethylene further encourages deterioration or senescence. The extent to which each of these processes occur depends generally upon both the concentration of ethylene present and the duration of ethylene exposure (7). The term "concentration" refers to the partial pressure of a particular gas in a gas solution.

Plants are often categorized according to the amount of ethylene they naturally release. For example, "very low" ethylene releasing plants release less than 0.1 microliters ethylene per kilogram per hour at 20°C, while "very high" ethylene releasing plants release greater than 100 microliters (or 1 milliliter) ethylene per kilogram per hour at 20°C. The rate at which a plant develops will be faster in a confined and/or poorly-ventilated space than in an unconfined and/or well-ventilated space. In a confined space, the concentration of ethylene present will likely increase before it can decrease. On the other hand, in an unconfined space, the concentration of ethylene present will likely decrease before it can increase (7). Ethylene's odor is typically only recognized by those who have handled ethylene before. The most common route of ethylene entry in humans

occurs via inhalation (5). Adverse health effects occur when the amount of oxygen in the air displaced by ethylene approaches 20% by volume or more (4, 8). Furthermore, ethylene gas is flammable at concentrations between 27,000 - 360,000 parts per million (ppm) or 2.7 - 36.0% by volume in air; therefore, advanced techniques that enable reliable detection and accurate measurement of ethylene gas are of great importance from a medical point-of-view, in agriculture, or in any other industrial or laboratory setting where ethylene is handled (8).

1.3: Overview of current trace gas detection techniques

Traditional trace gas analysis techniques include, but are not limited to, Fourier transform infrared spectroscopy (FT-IR), non-dispersive IR spectroscopy, and various gas chromatography-based techniques (9). Very few techniques are both portable enough for use outside of the laboratory setting and precise and accurate enough for reliable detection and measurement at preferably low concentrations (2). In a recent study, three techniques considered for use in fruit supply chains were employed to detect and measure the concentration of various samples of the chemical ethylene. These three techniques, which included non-dispersive IR spectroscopy, miniaturized gas chromatography, and electrochemical measurement, each presented their own unique advantages and disadvantages rendering neither one optimal for use. Specifically, among the three techniques considered, advantages of non-dispersive IR spectroscopy, miniaturized gas chromatography, and electrochemical measurement included relatively fast measurement, good accuracy, and high resolution, respectively. On the other hand, disadvantages of non-dispersive IR spectroscopy, miniaturized gas chromatography, and electrochemical measurement included relatively poor sensitivity, slow measurement, and high cost, respectively (4). Therefore, there exists a need for some other more advantageous trace ethylene detection technique.

1.4: Introduction to photoacoustic spectroscopy as an effective trace gas detection technique

Photoacoustic (PA) spectroscopy refers to the application of the PA effect for spectroscopic purposes (9). This phenomenon, first discovered in 1880, grew in popularity nearly half a century after its initial discovery upon discovery of the microphone and laser (10). The PA effect can be summarized into the following three major steps: the localized release of heat from a sample of gas within a cavity resonator, the generation of acoustic waves due to this release of heat, and the detection and measurement of the acoustic signal produced (9, 10). How the PA effect occurs is explained in further detail in Chapter 2: Background.

This technique is especially useful for detecting and measuring the concentration of strongly absorbing gases, or gases with high absorption coefficients. Recent research on the PA effect of sulfur hexafluoride, SF_6, revealed that standing waves within a cavity resonator had different amplitudes at different microphone positions (11). Furthermore, it was determined that the modulation frequency at which PA resonance occurs for sulfur hexafluoride varied depending upon the internal length of the cavity resonator, the temperature within the cavity resonator, and the concentration of the gas sample contained within the cavity resonator expressed as a function of the molecular mass of the gas solution (12).

1.5: Statement of intent

Compared with more traditional spectroscopic and trace gas analysis techniques, knowledge of the use of PA spectroscopy as an effective technique for chemical analysis appears far less widespread among chemists and bio-environmental scientists. There is even less

documentation addressing the PA behavior of the plant hormone ethylene. This project seeks to contribute to the current understanding of the PA effect of ethylene gas by identifying how various facets of this technique can be manipulated to enhance its usability.

In this research project, various aspects of the experimental setup in this research project will be independently manipulated to determine each of their effects on the PA signal produced by ethylene. These aspects include the internal diameter of the cavity resonator, power of the light source, concentration of analyte gas contained within the cavity resonator, and rotational frequency of the mechanical chopper. Furthermore, the dimensions of the cavity resonator will be manipulated to determine whether the detection limit of ethylene is affected as a result.

Theory found in physical and online references paired with data obtained in the UTC Department of Chemistry and Physics research laboratory will be used to help formulate a discussion about the PA effect of ethylene gas. By better understanding the experimental conditions that best enable precise and accurate measurements of ethylene, manufacturers can better create highly-sensitive, low-cost, portable systems that can still deliver reliable continuous measurements both inside and outside of the traditional laboratory setting.

Chapter 2: Background

Table of Contents

2.1: History of photoacoustic effect

The PA effect was discovered by Alexander Graham Bell in 1880 when he noticed that thin discs exposed to a rapidly interrupted beam of light produced sound. In a later experiment, Bell placed absorbing substances inside a spectroscope at the focal point and observed sound in all parts of the sun's electromagnetic spectrum using a hearing tube (2). Through his experiments, Bell proposed that gas, liquid, and solid materials exposed to modulated radiation produced acoustic waves that could be both detected and measured (11). Due to the lack of a proper light source, microphone, and electronics, the PA effect was left unstudied for nearly half a century (10). Few advancements in the study of the PA effect were observed during this time until the discovery of the microphone in 1938 and the laser in the 1960s (13, 2). The discovery of the laser brought

about improved beam quality, spectral purity, and power (in comparison to other conventional light sources) (10). Scholars Kerr and Atwood were among the first to combine laser technology with the PA effect to obtain absorption spectra of small gas molecules in the late 1960s (2). Scholars Kreuzer and Patel both incorporated this phenomenon into their studies of gases in the early 1970s (14). Using an IR Ne-He laser (3 μm), Kreuzer was able to detect and measure concentrations of methane gas in nitrogen gas to 10 parts per billion (ppb). Patel was able to detect and measure concentrations of nitrogen monoxide and water at high altitudes using a balloon-borne spin-flip Ramen laser. Other noteworthy scholars that contributed to today's understanding of the PA effect include scholars Röntgenx, Tyndall, Preece, Viegerov, and Luft. Recent advancements in the PA research include applications of trace gas detection for environmental, biological, and medical purposes (2).

2.2: Breakdown of photoacoustic spectroscopy

Photoacoustic spectroscopy refers to the application of the PA effect for spectroscopic purposes (9). The mathematical theory behind the PA effect is complicated, yet the effect, itself, can be summarized into the following three major steps: the localized release of heat from a sample of gas due to the excitation and subsequent de-excitation of the sample's internal energy levels, the generation of acoustic waves due to this heat release, and the detection and measurement of the acoustic signal produced within a cavity resonator using a microphone (9, 10).

Electromagnetic radiation in the form of photons, or massless particles containing energy, is emitted from a continuous-wave light source and directed through the window of a cylindrical cavity resonator (14). This radiation must have a wavelength that falls within the range of wavelengths permitted by the window; otherwise, the radiation will not be able to enter the cavity

resonator and the PA effect will not be observed (12). Prior to entering the cavity resonator, the radiation emitted from the light source is modulated using a mechanical chopper together with a frequency modulator. The frequency at which this mechanical chopper rotates can be set and adjusted using the frequency modulator (10). Using the frequency modulator, the rotational frequency of the mechanical chopper can range anywhere from single value to several thousand hertz (Hz) (15). As the radiation emitted from the continuous-wave light source passes through the rotating mechanical chopper, the radiation is modulated or intermittently broken up at a frequency proportional to the rotational frequency of the mechanical chopper (10). Upon entering the cavity resonator, photons emitted from the light source can strike the analyte gas molecules contained within. The absorption of the incident photons by the analyte gas molecules causes the internal energy levels within the sample to become excited to a higher quantum state. The de-excitation of these internal energy levels within the sample can occur via radiative or non-radiative processes. The excitation and de-excitation of the internal energy levels occur at a frequency influenced by but not directly proportional to the rotational frequency of the mechanical chopper (16). The frequency at which the internal energy levels become excited and de-excited cannot be directly proportional to the rotational frequency of the mechanical chopper due to the fact that the frequency at which the excitation and de-excitation takes place is several orders of magnitude greater than any rotational frequency that a mechanical chopper can achieve. Radiative processes include spontaneous or stimulated emission, while non-radiative processes include intermolecular collisions (16). Radiative relaxation processes will not be discussed in this thesis. Non-radiative relaxation to the ground state via intermolecular colliding results in the transformation of energy lost into translational kinetic energy. This loss of energy presents in the form of heat. Thermal changes in an isochoric system in which the volume remains constant results in pressure change

(15). The intermittent excitation and de-excitation of the internal energy levels causes fluctuations in pressure within the cavity resonator (17). These pressure fluctuations are the direct result of force (in the form of mechanical waves) being generated as the analyte gas molecules seek to minimize the localized stress caused by the subsequent excitation and de-excitation of their internal energy levels. (13). These fluctuations in pressure present in the form of measurable infrasonic, audible, or ultrasonic waves that can be detected and transduced, or converted from one form into another, using a microphone. At any point in time, these mechanical waves traverse along longitudinal eigenmodes, along radial eigenmodes, or both. At modulation frequencies below 1 Hz, these pressure fluctuations manifest in the form of infrasonic waves; at modulation frequencies between 16 Hz and 16 kHz, these pressure fluctuations manifest in the form of audible waves, and at modulation frequencies greater than 16 kHz, these pressure fluctuations manifest in the form of ultrasonic waves (13).

In PA spectroscopic experiments, microphones are used as a type of piezoelectric transducer. These types of transducers are capable of converting mechanical fluctuations or changes in physical quantities to electrical signals that can be observed using the proper electronics. As the microphone picks up acoustic waves generated within the cavity resonator, it converts these mechanical fluctuations into electrical signals that manifest as a visible waveform that can be seen using an oscilloscope and heard using a speaker (11). This waveform has an amplitude proportional in magnitude to the number of incident photons absorbed by the analyte gas which may depend upon the number of analyte gas molecules contained within the cavity resonator—expressed as a particular concentration of analyte gas—when the number of incident photons entering the cavity resonator is kept constant, or it may depend upon the number of incident photons entering the cavity resonator—expressed as the power of the light source emitting the

photons—when the number of analyte gas molecules contained within the cavity resonator is kept constant. As previously mentioned, the word "concentration" refers to the partial pressure of a particular gas in a gaseous solution held at some arbitrary total pressure. Throughout this research project, the word "concentration" was used to describe the amount of analyte gas, or the partial pressure of the analyte gas, contained within a cavity resonator. In an isochoric system, the sum of the partial pressures of the analyte gas and the buffer gas equals the total pressure within the cavity resonator. For example, an analyte-buffer gas solution with an analyte gas concentration of 25% by volume will have enough analyte gas to contribute 25% towards the total pressure within the cavity resonator and enough buffer gas to contribute the remaining 75% towards the total pressure. In this case, if the total pressure within the cavity resonator is 1.0 atmosphere (atm), the partial pressure of the analyte gas will be 0.25 atm, and the partial pressure of the buffer gas will be 0.75 atm.

The typical waveforms of a PA signal (shown as an orange/yellow waveform) and the typical waveform of a reference signal (shown as a blue waveform) can both be found in Figure I.

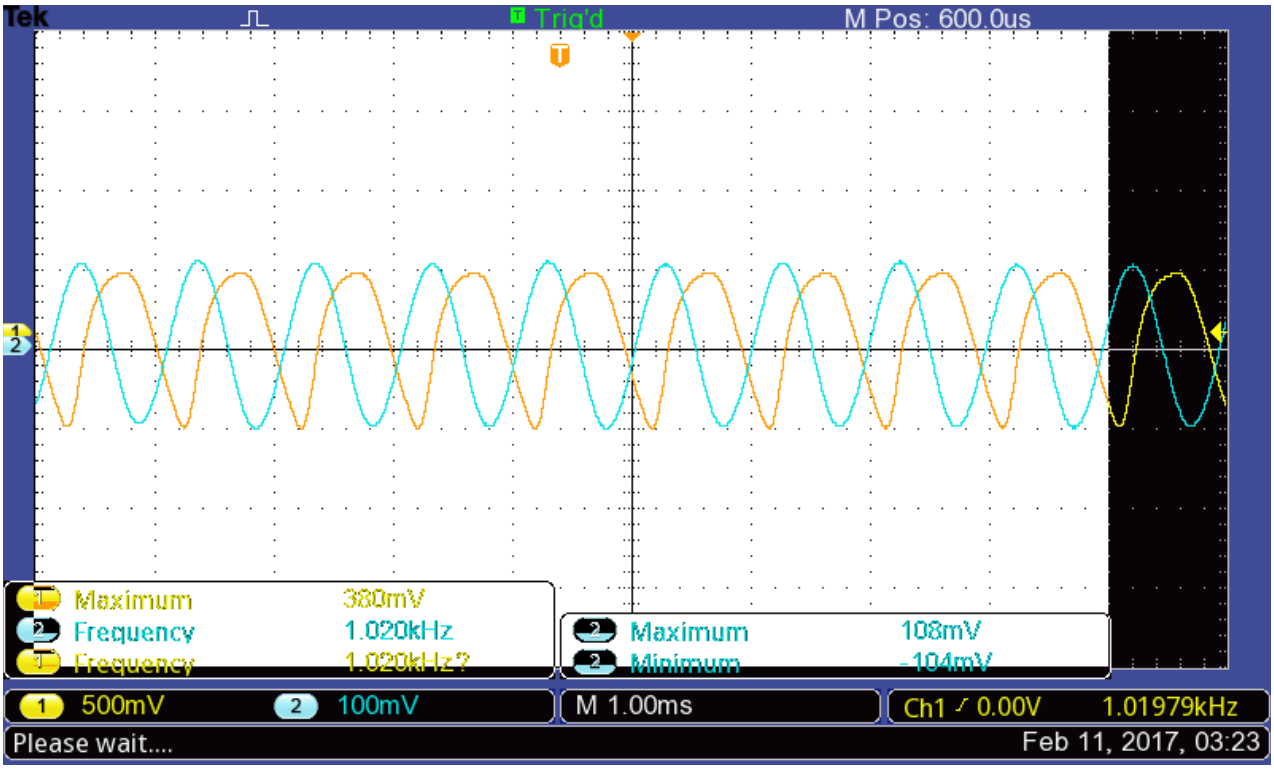

Figure I. Typical waveforms of a photoacoustic signal and reference signal

The amplitude of the waveform shown on the oscilloscope, also referred to as the intensity of the PA signal, is proportional in magnitude to the power of the light source according to Equation I where the variable p_0 represents the acoustic pressure amplitude (in N m^{-2}), the variable P represents the power of the light source (in W), and the variable γ represents the optical absorption coefficient (in m^{-1}) (12).

$$Equation\ I. p_0 const \propto \gamma P$$

The Resonance Frequency Equation is shown below in Equation II where the variable f_{res} represents the resonance frequency or modulation frequency at which resonance occurs (in Hz), the variable C_s represents the speed of sound (in cm/s), the variable γ represents the optical

absorption coefficient unique to the analyte gas under consideration, the variable R represents the gas constant, the variable L represents the internal length of the cavity resonator (in cm), the variable T represents the temperature (in K), and the variable M represents the relative concentration of the analyte-buffer gas contained within the cavity resonator expressed as the theoretical molecular mass of the analyte-buffer gas (in amu). For an analyte-buffer gas solution containing ethylene gas (analyte) and nitrogen (buffer), the value of M falls within the range of 28.0532 amu (molecular weight of ethylene) and 28.01345 amu (molecular weight of nitrogen). The exact value of M depends upon the relative abundances of both the analyte gas and buffer gas solutions.

$$Equation\ II.\ f_{res} = C_s\left(\frac{1}{2L}\right) \propto \sqrt{\frac{\gamma RT}{M}} \times \left(\frac{1}{2L}\right)$$

Additionally, the amplitude of the pressure fluctuations will be greater in a closed cavity resonator than the amplitude of the pressure fluctuations in an open cavity resonator due to enhanced constructive interference of the mechanical waves (10). Maximum amplitudes, or waveforms with relatively large amplitudes, for the acoustic waves generated occur at specific resonance frequencies within the cavity resonator (10). In PA spectroscopy, resonance occurs when the frequency of the pressure fluctuations reflected off the boundaries of the cavity resonator at an arbitrary point in time is in phase with the natural frequency of the pressure fluctuations generated by the photon absorption of the analyte gas molecules at another arbitrary point in time (11, 13). When these two frequencies are in phase with one another, the resulting superimposed mechanical wave is detected by the microphone and transduced into a waveform with a relatively large

amplitude. For an isochoric system, the frequency and magnitude of the pressure fluctuations generated by the analyte gas molecules will depend upon the rotational frequency and duty cycle, respectively, of the mechanical chopper.

Again, a continuous-wave light source and a mechanical chopper together with a frequency modulator are typically employed in PA spectroscopy; however, the radiation may also be pulsed (versus modulated) by the light source, itself, prior to entering the cavity resonator. At low modulation frequencies and pulsation frequencies, the excited internal energy levels of the analyte gas molecules will have more time to relax back down to the ground state before being re-excited upon reabsorption of photons from the light source. The resulting pressure fluctuations will, therefore, be well-separated both in time and in space. As the modulation frequency and pulsation frequency increases, the time in between each consecutive excitation and de-excitation decreases, resulting in pressure fluctuations that are more difficult to distinguish among one another (17). This phenomenon can be attributed to the fact that heat pulses last somewhat longer than the light pulses; in other words, the amount of time it takes for the internal energy levels to relax back down to the ground state is typically longer than the amount of time it takes for the internal energy levels to become excited in the first place (10). With modulated radiation, the gas molecules contained within the cavity resonator spend as much time exposed to the photons from the light source as they do shielded from the photons, resulting in a 50% duty cycle. With pulsed radiation, the gas molecules spend more time shielded from the photons than they do exposed, resulting in a lower duty cycle (17). At very low duty cycles, the resulting pressure fluctuations will also be well-separated in time and in space but small in magnitude, while at very high duty cycles, the resulting pressure fluctuations will be poorly-separated. Analyte gas molecules exposed to radiation with a

50% duty cycle will result in pressure fluctuations that are both well-separated and large in magnitude (10).

An analysis of the PA effect of any sample reveals information about the transient flow of heat to and from that sample. It can be argued that application of the PA technique is as much a form of calorimetry as it is a form of optical absorption spectroscopy (9). A gas solution with a high concentration of analyte gas molecules will absorb more photons, release more heat, and thus generate larger pressure fluctuations than a gas solution with a relatively lower concentration of analyte gas molecules, which will absorb less photons, release less heat, and thus generate smaller pressure fluctuations. PA spectroscopy can, therefore, be used to measure the concentration of any analyte gas molecule contained within a gas solution.

2.3: About ethylene

Dimitry Nikolayevich Neljubov, a researcher at the Botanical Institute in St. Petersburg, discovered ethylene in the 19th century when he noticed this gaseous chemical caused his pea seedlings to grow horizontally, making it the first phytohormone ever identified. The rise of gas chromatography technique in the late 20th century brought about increased awareness and respect for ethylene as a self-regulator of plant growth and development (6). This phytohormone has been known to help regulate seed germination, the adjustment of seedlings to soil conditions, color change, degreening of citrus fruits, and the development, senescence, and abscission of leaves (6, 7). Negative effects of ethylene often include reduced storage life, increased oxidative browning, and quickened senescence. More specific adverse effects of ethylene include the formation of bitter-tasting chemicals in carrots, russet spotting on lettuce, and inhibited blooming of carnations (7).

Naturally, ethylene is generated by plants metabolically via the conversion of S-adenosyl-L-methionine (SAM) into ethylene through the methionine cycle. There are two catalysis reactions involved in this process. First, SAM is converted into the cyclic amino-acid intermediate 1-aminocyclopropane-1-carboxylic acid (ACC) using the enzyme ACC synthase. Finally, ACC is converted into ethylene (with cyanide as a byproduct) using the enzyme ACC oxidase (6, 7).

In addition to its natural occurrence and use as a plant hormone, ethylene, formerly used as an anesthetic, is also used as a refrigerant and in the production of alcohol, mustard gas, petrochemicals, polymers, and resins. This chemical is a common air contaminant found in tobacco smoke, automative and diesel exhaust and is produced via the manufacturing of petroleum (5).

This colorless, flammable gas has a slightly sweet odor that is generally only recognized by those who have had experience handling ethylene before. At extremely low temperatures, ethylene may also exist as a colorless liquid (8). Ethylene is often referred to as acetene, ethene, olefiant gas, and bicarburretted hydrogen as well. Each molecule consists of two double-bonded carbons with two hydrogens attached to each carbon (5). Ethylene has a molecular mass of 28.05 amu (4). The specific weight of ethylene gas (1.1718 kg/m^3 at 15°C) is similar to that of air (1.225 kg/m^3 at 15°C), thus making it possible for ethylene gas to dissipate evenly in air. The ability of ethylene gas to dissipate evenly in air can be both useful or harmful, depending on the setting. Free-flowing distribution of ethylene gas into large, open, or well-ventilated spaces like stores can induce the slow and even ripening of fruits and vegetables, while free-flowing distribution of gas in small, closed, or poorly-ventilated spaces like ships and trucks can force fruits and vegetables to ripen too quickly and unevenly (4). Fruits and vegetables are often categorized according to the amount of ethylene they naturally release. Fruits and vegetables that release less than 0.1 microliters ethylene

per kilogram per hour at 20°C, including cherry, citrus, artichoke, and asparagus, are considered "very low" ethylene releasers; between 0.1 and 1.0 microliters ethylene per kilogram per hour are considered "low"; between 1.0 and 10.0 microliters ethylene per kilogram per hour are considered "moderate"; between 10.0 - 100.0 microliters ethylene per kilogram per hour are considered high; fruits and vegetable that release greater than 100.0 microliters ethylene per kilogram per hour are considered "very high" ethylene releasers (7).

Inhalation is the most common route of ethylene entry in humans (5). Ethylene's ability to travel across both short and long distances may pose serious health risks to humans if the amount of oxygen in the air displaced by the ethylene gas, a simple asphyxiant, approaches 20% by volume or more (4, 8). Though ethylene has a relatively short half-life of 1.9 days (5), acute overexposure to ethylene gas has been linked to numerous respiratory and non-respiratory symptoms in humans. These symptoms include, but are not limited to, headache, ringing in the ears, dizziness, drowsiness, unconsciousness, nausea, and vomiting (8). It is worth noting that the majority of ethylene inhaled is exhaled before it can enter the bloodstream. Presently, there are no known adverse health effects linked directly to chronic exposure to ethylene gas; however, chronic exposure to oxygen-deficient environments can cause decreased alveolar partial oxygen pressure and induce hypoxemia, which has been linked to numerous symptoms associated with the cardiac and central nervous system (5, 8). These symptoms include, but are not limited to, central nervous system depression, unconsciousness, and even death. In severe cases, acute respiratory distress syndrome (ARDS) and/or other acute and potentially life-threatening lung injuries may develop. The signs and symptoms for these conditions may not develop for at least 24 hours but usually by 72 hours. Contact exposure of liquid ethylene to human skin can result in local frostbite at the site of contact and other forms of skin irritation, while contact exposure to the eyes can cause redness

and burning. Entry of ethylene gas in humans via ingestion can lead to irritation of the gastrointestinal tract; however, toxicologically significant levels of ethylene rarely are absorbed by the digestive tract (5).

It is, therefore, imperative that ethylene in both its gas and liquid form be handled with caution. Ethylene should be stored in unconfined and/or well-ventilated spaces as a precautionary measure to prevent the build-up of ethylene gas to potentially explosive concentrations. In the event of a cylinder leak that cannot be sealed, sources of ignition should be shut off, the area should be evacuated, and the cylinder should be relocated to an open-air space and emptied (5).

The slightly sweet odor of ethylene can be detected by humans between concentrations of 260 - 4000 ppm, rendering odor, alone, an unreliable indicator of possible overexposure to ethylene (5). *In situ* measurements of ethylene concentration outside of the laboratory are difficult to perform due to the lack of a portable yet sensitive unit capable of accurately and repeatedly detecting at preferred resolutions of a few ppb. Therefore, presently, measurements of ethylene concentration are performed using stationary equipment found in laboratories or in other similar environments (4).

Chapter 3: Materials and Methodology

Table of Contents

3.1: Materials

The terms "PA cell" and "PA detector" are often used interchangeably. The two terms, however, do not refer to the same thing. The PA cell includes those components that make up the acoustic unit. This acoustic unit includes an analyte gas, a buffer gas, a cavity resonator, a pair of windows, and a microphone. On the other hand, the PA detector includes all components that make up the instrument. In addition to those components that make up the acoustic unit, the PA detector includes a light source, a gas handling system, and any electronics necessary for gas detection (10).

A general overview of the experimental setup used in this research project is displayed in Figure II. The physical setup of the PA detector consisted of the following components: a gas cylinder containing the analyte gas, a gas cylinder containing a buffer gas, a cavity resonator with a gas inlet and outlet, a pair of windows, a microphone together with a compatible power source and voltage amplifier, an oscilloscope, a light source together with a compatible controller, a thermal power sensor together with a compatible power and energy meter console, a reference laser, a photodetector, and a mechanical chopper together with a frequency modulator. Additionally, Parafilm M® All-Purpose Laboratory Film, hereafter referred to simply as Parafilm, was used in the assembly of the cavity resonator and in the attachment of the microphone to the cavity resonator, sleeve rubber stoppers were used to seal the gas inlet and outlet, an IR spectrometer was used to obtain the IR spectra of both the analyte gas and the buffer gas, and a balloon, clamp, syringe, and rubber hose were used to dispense controlled volumes of gas into the cavity resonator.

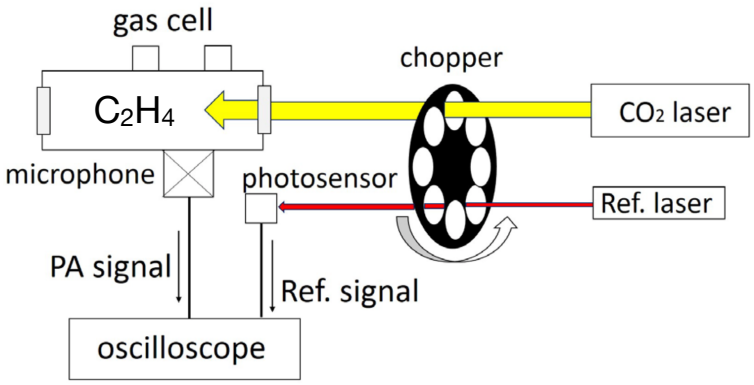

Figure II. General overview of experimental set-up

In this research project, pure ethylene gas was used as the analyte gas and nitrogen gas was used as the buffer gas. Both gases were contained within gas cylinders throughout the research period at some unknown pressure greater than 1 atm. The Chemical Abstracts Service registry number for ethylene is 74-85-1 (8). The Chemical Abstracts Service registry number for nitrogen is 7727-37-9 (18). Nitrogen gas was selected for use as a buffer gas for two reasons: its ability to evenly dissipate in ethylene gas and because it is a non-IR-absorbing gas. (19). Nitrogen, which presents as diatomic nitrogen gas in its elemental form, has a molecular mass of 28.01 amu and a specific weight of 1.153 kg/m^3 at 15°C (18). Ethylene, as previously-mentioned, has a molecular mass of 28.05 amu and a specific weight of 1.178 kg/m^3 at 15°C (4). Nitrogen, therefore, is capable of dissipating evenly both in ethylene gas and in air.

In this research project, three glass cavity resonators with gas inlets and outlets were used to hold gas solutions containing both buffer gas and analyte gas. Windows were attached to both ends of the cavity resonators using Parafilm, and sleeve rubber stoppers were inserted into both the gas inlets and the gas outlets. Additionally, Parafilm was used to modify the geometries of the cavity resonators and to attach the microphone to the cavity resonators. The use of windows, sleeve rubber stoppers, and film allowed for the construction of almost entirely closed-off cavity resonators with defined volumes. The most common cavity resonators used in PA spectroscopy are shaped like cylinders because the symmetry of a cylindrical cavity resonator coincides best with the laser beam's direction of propagation (10). The three different cylindrical cavity resonators possessed their own unique internal radii, internal lengths, and internal volumes and were constructed using various apparatuses. Note that the various apparatuses used to construct each cavity resonator were not specifically designed to be used in PA spectroscopy research; therefore, the three cavity resonators used in this research project were not perfectly cylindrical—the cavity

resonators were irregularly shaped. The internal radii, internal lengths, and internal volumes for the first cavity resonator, hereafter referred to as "Cell 1," the second cavity resonator, hereafter referred to as "Cell 2," and the third cavity resonator, hereafter referred to as "Cell 3," can be found in Table I.

Table I. Dimensions of the cavity resonators

Cell #	Internal Length (cm)	Internal Radius (cm)	Internal Volume (mL)
1	45.0	0.953	95.3
2	44.0	1.91	341.8
3	45.0	2.54	649.0

The internal radius of each cavity resonator was measured at each of their widest points. The internal length of each cavity resonator was measured from one end of the cavity resonator to the other, excluding the additional lengths of each window. The internal volume of Cell 1 was approximated by enclosing the cavity resonator but leaving either the gas inlet or gas outlet open, completely filling the cavity resonator with tap water through either the gas inlet or gas outlet, transferring the water from the cavity resonator to a graduated cylinder (or multiple graduated cylinders if needed), and measuring the volume of water to one decimal places (no approximation of the second decimal place). As previously-stated, the use of windows, sleeve rubber stoppers, and Parafilm allowed for the construction of an almost entirely closed-off cavity resonator with a defined volume. Because the cavity resonators used in this research project were irregularly shaped, the geometry of each cavity resonator was modified as needed using Parafilm to form the desired cylindrical shape. Measurements of the internal volume of Cell 1 were repeated twice more for a total of three trials. The mean of these three measurements was calculated to determine the best

approximation for the internal volume of Cell 1. This process was repeated twice more using the other two cavity resonators to determine the best approximation for the internal volumes of Cell 2 and Cell 3. An image of Cells 1, 2, and 3 can be found below in Figures III, IV, and V, respectively.

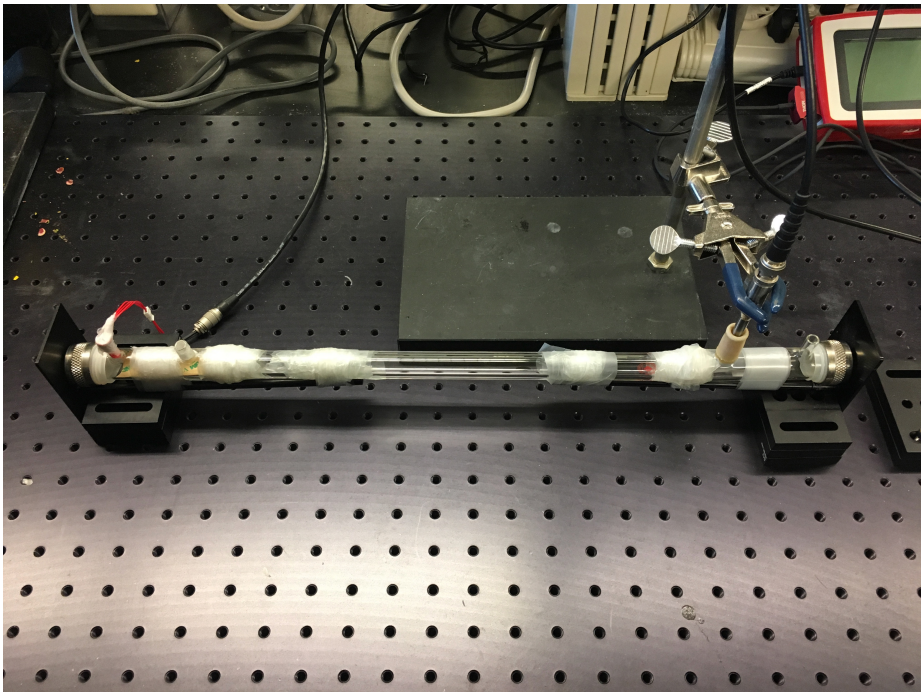

Figure III. Image of Cell 1

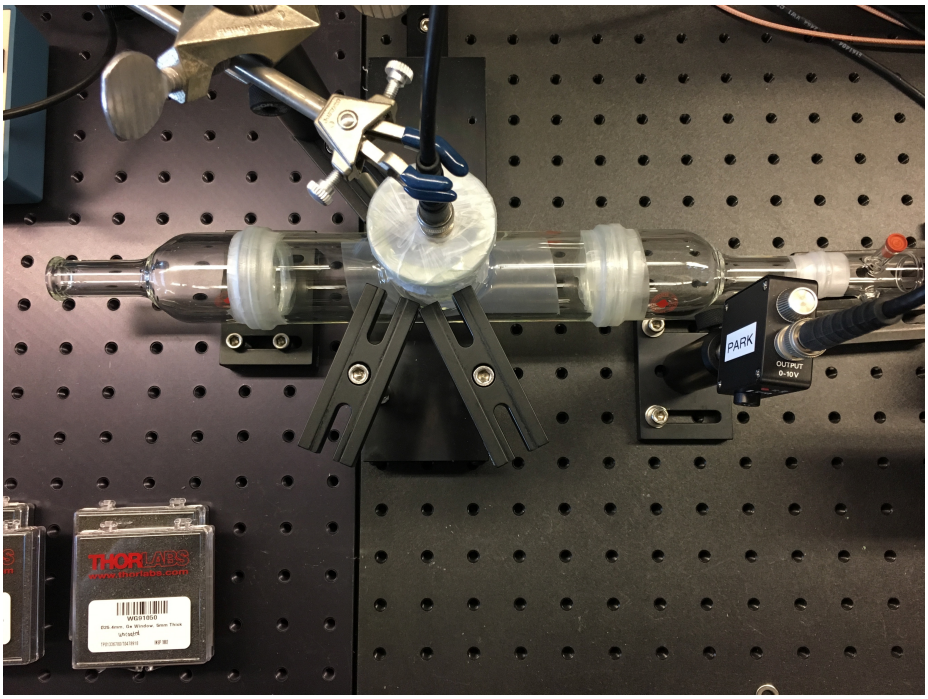

Figure IV. Image of Cell 2

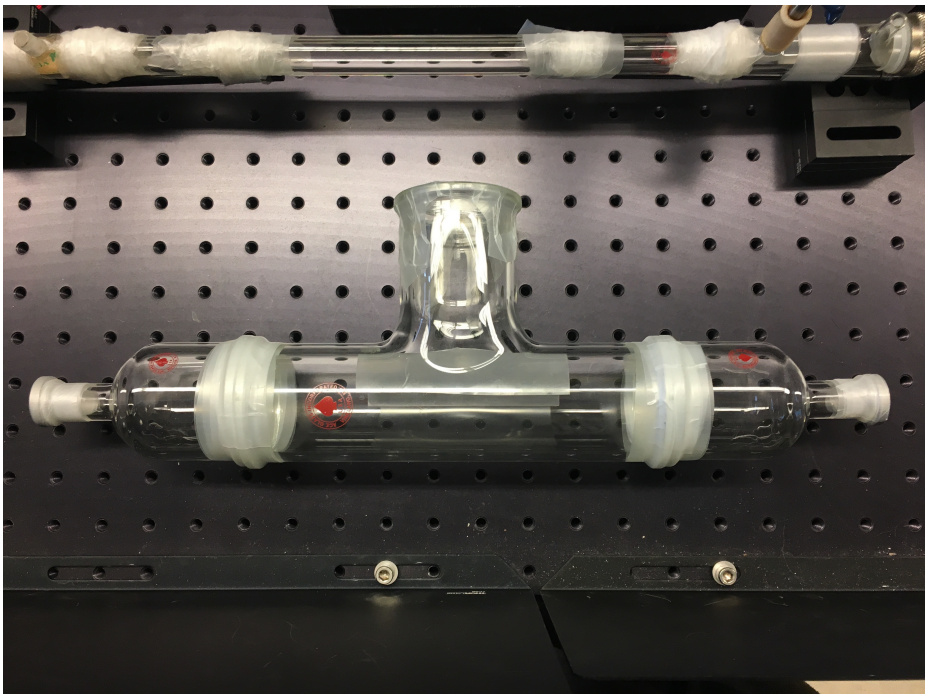

Figure V. Image of Cell 3

Additionally, a fourth cavity resonator with a gas inlet and gas outlet, hereafter referred to as "Cell 4" was used in select experimental runs when using neither Cell 1, Cell 2, nor Cell 3 were neither necessary nor appropriate. Sleeve rubber stoppers and a set of windows were also used with Cell 4 to allow for the construction of an almost entirely closed-off cavity resonator with a defined volume (though the specific measurements for the internal length, internal radius, and internal volume of this particular cavity resonator were not of significance in this research project).

In this research project, two different sets of windows were used. Windows were used to enclose the cavity resonator and to filter the radiation that was emitted from the light source as it entered the cavity resonator. Ethylene is IR-active at wavelengths around 10.6 μm and, therefore, will only absorb photons with wavelengths at or around 10.6 μm. This IR-activity around the wavelength 10.6 μm corresponds to a vibrational mode that occurs around the frequency 943 cm^{-1}. At this frequency, a CH_2 wag will occur. It is, therefore, necessary that the windows used in this research project also be capable of transmitting radiation at or around this wavelength. If the radiation emitted from the light source does not have a wavelength that falls within the range of wavelengths permitted by the window, the PA effect will not be observed. The first set of windows used in this research project (model number, WG91050) were not coated with an antireflective coating, while the second set of windows (model number: WG91050-G) were coated with an antireflective coating. Both sets of windows were one inch diameter windows manufactured out of the chemical germanium (Ge) and produced by ThorLabs, Inc. Both sets of windows allowed the transmission of radiation between the wavelengths of 7 - 12 μm. The antireflective coating applied to the Ge windows was designed to reduce the average reflectance of the incident radiation hitting the coated Ge window to less than one percent when compared to the incident radiation hitting an uncoated Ge window. The percent transmittance was approximated for both the set of uncoated

Ge windows and the set of coated Ge windows to determine whether the difference between the percent transmittance for the set of coated windows and the percent transmittance for the set of uncoated windows was great enough to justify the additional expense required to obtain these windows. To determine the percent transmittance for the set of uncoated windows, one uncoated window was first attached to one end of Cell 4. The cavity resonator was placed directly in front of the CO_2 laser—this light source will be described in further detail later—so that the radiation's direction of propagation was perpendicular to the surface of the window. Using the thermal power sensor together with the power and energy meter console—both of which will also be described in further detail later—the output power was measured when the thermal power sensor was placed between the cavity resonator and the CO_2 laser and when the thermal power sensor was placed behind the cavity resonator. These two measurements allowed us to directly compare the power of the radiation that reached the thermal power sensor with and without transmittance through the window. The two aforementioned measurements were obtained for the one uncoated window when the controller—to be described in further detail later—was set to emit a radiation at 100% of its maximum output power, 75% of its maximum output power, 50% of its maximum output power, and 25% of its maximum output power. A simple calculation was performed to approximate the percent of the radiation emitted from the light source that actually transmitted through the window and reached the thermal power sensor. The previously-described process was repeated once more to obtain a second approximation for the percent transmittance for the uncoated window and repeated two additional times using one of the coated windows to approximate the percent transmittance for the set of coated windows used in this research project. The approximations for the percent transmittances of the set of uncoated windows and the set of coated windows were determined to be 25.5% and 85.74%, respectively, using Equation III shown

below where the variable %T represents the percent transmittance, the variable P_i represents the power of the radiation that reached the thermal power sensor without initial transmittance through the window, and the variable P_f represents the power of the radiation that reached the thermal power sensor with initial transmittance through the window.

$$Equation\ III.\ \%T\ = 100(\frac{P_i}{P_f})$$

Based off this preliminary data, it was determined that the difference between the percent transmittance for the set of coated windows and the percent transmittance for the set of uncoated windows was, in fact, great enough to justify the additional expense required to obtain these values. The set of coated Ge windows were used throughout the remainder of the research project.

In this research project, a microphone with a built-in voltage amplifier together with a compatible power source and an oscilloscope were used to detect and to convert the acoustic waves generated within the cavity resonator into visible waveforms that can be seen using an oscilloscope and heard using a speaker. The microphone used in this research project served as a type of integrated circuit piezoelectric (ICP) transducer. As previously stated in Chapter 2, these types of transducers are capable of converting changes in physical quantities into electrical signals that can be observed using the proper electronics. Parafilm was used to position the microphone into each of the three cavity resonators. The microphone used is a ICP Electret Array Microphone (model number: 130E20) produced by PCB Piezotronics. The power source for the ICP transducer used is a battery-powered signal conditioner for ICP sensor (model number: 480C02) produced by PCB Piezotronics. The oscilloscope used in this research project is a digital oscilloscope (model number: TBS 1202B) produced by Tektronix.

In this research project, a light source together with a compatible controller and a thermal power sensor together with a compatible power and energy meter were used to excite the internal energy levels of the analyte gas molecules and to measure the power of the radiation emitted from the light source, respectively. Ethylene is IR-active and will only absorb photons with a wavelength at or around 10.6 μm (7). Therefore, it is necessary that the light source together with the controller be capable of emitting radiation at or around this same wavelength. The light source used was a low-power continuous-wave CO_2 laser (model number: L3) produced by Access Laser Company. This particular model is capable of emitting radiation at wavelengths between 10.3 - 10.8 μm. According to the manufacturer, the light source used in this research project is designed to have a maximum output power of 400 mW. However, it is believed that repeat use of this particular piece of laboratory equipment from previous research projects has forced the reduction of its maximum output power over time. The maximum output power of the CO_2 laser used in this research project was approximated by first placing the thermal power sensor (connected to the power and energy meter console) directly in front of the CO_2 laser. The CO_2 laser was turned on and set to maximum laser power. Using the thermal power sensor together with the power and energy meter console, the output power was measured every ten seconds for one hundred seconds. The mean of these ten measurements was calculated to determine the best approximation for the maximum output power. The approximation for the maximum output power for the particular light source used in this research project was calculated to be 291.0 mW. Calculations were performed to determine the exact power of the radiation being emitted from the light source when the CO_2 laser was set to emit approximately 25%, 50%, and 75% of its maximum output power. These powers were determined to be 72.80 mW, 145.6 mW, and 218.3 mW, respectively, by multiplying the maximum output power for the particular light source used in this research project by 0.25,

0.50, and 0.75. The thermal power sensor used was a thermal surface absorber (model number: S310C) produced by ThorLabs, Inc. This particular model is capable of detecting radiation at wavelengths between 0.19 - 25 μm. The power and energy meter console used in this research project was a compact power and energy meter console (model number: PM100D) produced by ThorLabs, Inc.

In PA spectroscopy, a reference laser and a photodetector were used to generate a noise-free signal that could be observed on the oscilloscope. This waveform was used to help visualize changes in the PA signal caused by the interaction of the analyte gas molecules with the photons emitted from the previously-mentioned continuous-wave CO_2 laser. The reference laser used in this research project was a collimated laser diode module (model number: CPS182) produced by ThorLabs, Inc. The photodetector used in this research project was a high-speed silicon photodetector (model number: DET36A) produced by ThorLabs, Inc.

A mechanical chopper together with a frequency modulator was used to modulate both the radiation emitted from the light source and the radiation emitted from the reference laser. As the radiation emitted from the continuous-wave light source passed through the rotating mechanical chopper, the radiation was intermittently broken up at a rate proportional to the rotational frequency of the mechanical chopper. The mechanical chopper used in this research project was a 100-slot blade (model number: MC1F100) produced by ThorLabs, Inc. The frequency modulator used in this research project was an optical chopper system (model number: MC2000B) produced by ThorLabs, Inc. Together, the particular mechanical chopper and frequency modulator used in this research project were capable of modulating the radiation at frequencies between 200 Hz and 10,000 Hz.

Finally, an IR spectrometer was used to verify the absorption wavelengths for both the analyte gas and buffer gas. The IR spectrometer used in this research project was a FT-IR spectrometer (model number: Nicolet 380) produced by Thermo Scientific.

3.2 Methodology

In this research project, the following aspects of the experimental setup were intentionally and independently manipulated to determine each of their effects on the PA signal produced by ethylene gas: internal radius of the cavity resonator, power of the light source, concentration of analyte gas contained within the cavity resonator, and rotational frequency of the mechanical chopper. As previously-mentioned, each cavity resonator used in this research project was constructed using various apparatuses not specifically designed for use in PA spectroscopy experiments. Thus, it should be noted that experimental runs involving direct manipulation of the internal radius of the cavity resonator yielded data were influenced by indirect manipulation of the geometry of the cavity resonator. The methodology used in this research project is described below in three parts. Part one describes how IR spectroscopy was used to verify that the absorption wavelength for the buffer gas selected for use in this research project neither included nor was around the same wavelength as the analyte gas. The second part describes how the four aforementioned aspects of the experimental setup were manipulated to determine each of their effects on the PA signal of ethylene. The third and final part of this research project was performed to determine how manipulating the dimensions of the cavity resonator affected the detection limit of ethylene.

3.2.1: Part 1: Infrared spectra for ethylene and nitrogen

In the first part of this research project, IR spectroscopy was used to verify the absorption wavelength of the analyte gas and to verify that the presence of the buffer gas used would not unintentionally interfere with the analyte gas's ability to absorb photons. The theoretical wavelength at which the analyte gas, ethylene, absorbs photons is 10.6 μm; therefore, it is necessary that the buffer gas either not be able to absorb IR radiation at all or absorb photons at a wavelength that neither includes nor is around 10.6 μm. As previously mentioned, nitrogen gas was selected to serve as the buffer gas because the theoretical molecular masses and specific weights of ethylene gas and nitrogen gas in their elemental forms were both similar and because of the characteristic inability of nitrogen gas to absorb IR radiation.

To obtain the IR spectrum of ethylene gas, the set of coated windows were first attached to both ends of Cell 4 and a sleeve rubber stopper was inserted into both the gas inlet and outlet. Using EZ Omnic software, the parameters of the Nicolet 380 FT-IR spectrometer were set to the following parameters: resolution = 1 cm^{-1}; number of scans = 16; file handling = save automatically; background handling = collect background after 60 seconds. The background spectrum was obtained for the cavity resonator containing no ethylene gas.

Afterward, one of the sleeve rubber stoppers was removed from either the gas inlet or gas outlet. The cavity resonator was completely filled with ethylene gas by connecting the gas cylinder containing pure ethylene gas to the open gas outlet (or inlet) using a rubber hose and allowing ethylene gas to freely flow into and throughout the cavity resonator for several seconds. A sleeve rubber stopper was inserted back into the open gas outlet (or inlet) to enclose the cavity resonator. Without changing the parameters of the FT-IR spectrometer, the sample spectrum was obtained for the cavity resonator containing the ethylene gas. The absorption wavelength of any given gas

does not depend on the concentration of the gas sample; in other words, the wavelength at which a particular gas within a cavity resonator absorbs photons will remain the same regardless of how much of that particular gas is present. Therefore, the exact concentration of the ethylene gas contained within the cavity resonator was not of significance in this research project, though it was assumed that any undesired residual gas was expelled upon free-flowing addition of ethylene gas into and throughout the cavity resonator.

The previously-described methodology for obtaining the IR spectrum of ethylene gas was repeated using nitrogen gas to obtain the IR spectrum for the buffer gas. Afterward, both spectra were compared with one another to verify that the absorption wavelength (if applicable) for the buffer gas selected for use in this research project neither included nor was around the same wavelength as the analyte gas.

3.2.2: Part 2: Experimental runs with manipulated parameters

In the second part of this research project, four aspects of the experimental setup were intentionally and independently manipulated to determine each of their effects on the PA signal of ethylene. These aspects include the internal radius of the cavity resonator, power of the light source, concentration of analyte gas contained within the cavity resonator, and rotational frequency of the mechanical chopper. The data obtained for each experimental run was plotted to create a spectrum. Afterward, all spectra were compared with one another and used to help formulate a discussion about what experimental conditions were ideal for detecting and accurately measuring the concentration of ethylene gas using PA spectroscopic technique.

For experimental runs involving cavity resonators with varying internal radii, the three cavity resonators, each with their own unique internal radii, were interchanged while the power of

the light source remained constant. The internal radii for Cells 1, 2, and 3 can be found in Table I. As each of the three cavity resonators were interchanged, they were placed directly in front of the CO_2 laser and oriented so that the radiation's direction of propagation was as aligned with the cavity resonator's axis of symmetry as possible. For each of the three cavity resonators, the rotational frequency of the mechanical chopper was manually increased from 200 Hz to 4000 Hz in order to determine the intensity of the PA signal due to the interaction of the analyte gas molecules with the photons emitted from the light source as the concentration of the analyte gas obtained within the cavity resonator was varied. The power of the light source remained constant for each of these experimental runs. The data sets obtained from each experimental run were used to create spectra of PA signal intensity (in mV) versus rotational frequency of the mechanical chopper (in Hz).

One experimental run was performed to determine what effect manipulating the power of the light source had on the intensity of the PA signal produced. To perform this experimental run, Cell 1, enclosed using sleeve rubber stoppers and the set of uncoated windows, was filled completely with ethylene gas to achieve a desired concentration of 100% analyte gas. (Note that for this particular experimental run, the set of uncoated windows was used. Because the percent transmittance for the set of uncoated windows was previously determined to be insufficient for use in this research project, the set of coated windows was used for all experimental runs described hereafter.) The rotational frequency of the mechanical chopper was arbitrarily set to 250 Hz. Using the controller for the CO_2 laser, the power of the light source was gradually increased from minimum output power to maximum output power while the concentration of the analyte gas contained within the cavity resonator and the internal radius of the cavity resonator remained constant. As the power of the light source was manipulated, the resulting intensity of the PA signal

produced by the ethylene gas (as shown on the oscilloscope) was recorded. The thermal power sensor together with the compatible power and energy meter console was used to measure the exact power of the radiation being emitted from the light source as the power of the light source was gradually increased using the controller. After recording the intensities of the PA signal as the output power of the light source was increased from 0% to 100% of its maximum output power, the intensities of the PA signal were adjusted to correct for any background signal that may have presented. The data set obtained was used to create a plot of PA signal intensity (in mV) versus laser power (in mW). For experimental runs involving a constant power of the light source, the CO_2 laser was set to emit radiation at its maximum power using the controller. As previously mentioned, the maximum output power for the particular light source used in this research project was experimentally-calculated to be 291.0 mW.

For experimental runs involving varying concentrations of analyte gas, each of the three cavity resonators were filled with pre-determined volumes of ethylene gas to produce analyte-buffer gas solutions with specific concentrations, represented as the percent of the internal volume of the cavity resonator that was displaced by analyte gas or the percent of the total pressure contributed by the analyte gas. For each of these experimental run, the power of the light source remained constant. Similarly as before, the rotational frequency of the mechanical chopper was manually increased from 200 Hz to 4000 Hz to determine the intensity of the PA signal under the unique conditions established for each particular experimental run. A series of calculations were performed to determine the volume of analyte gas that needed to be added to each cavity resonator in order to displace 5%, 10%, 25%, 50%, and 100% of the pre-existing gas in each cavity resonator. These volumes were determined by first approximating the internal volumes of Cells 1, 2, and 3 and then multiplying these volumes by 0.05, 0.10, 0.25, and 0.50. Prior to each

experimental run, nitrogen gas was circulated through the cavity resonator for several seconds to rinse the cavity resonator of all residual gas that may have been left behind by other laboratory personnel or from a previous experimental run. To rinse the cavity resonator, one of the sleeve rubber stoppers was removed from either the gas inlet or gas outlet. The cavity resonator was completely filled with nitrogen gas by connecting the gas cylinder containing pure nitrogen gas to the one gas outlet (or inlet) using a rubber hose and allowing nitrogen gas to freely flow into and throughout the cavity resonator for several seconds. To collect controlled volumes of analyte gas, a syringe was used to draw the desired volume of gas from a sealed balloon filled with ethylene gas. The pre-determined volumes of ethylene gas were then injected directly into the rinsed cavity resonator through a sleeve rubber stopper. The previously-described methodology was used to achieve desired concentrations of 5%, 10%, 25%, and 50%. It was assumed that 100% concentration of analyte gas could be obtained by allowing ethylene gas to freely flow into and throughout the cavity resonator. The pre-determined volumes of ethylene gas that needed to be added to each of the three cavity resonators to achieve desired concentration of 5%, 10%, 25%, 50%, and 100% are listed in Table II. It should be noted that the particular syringes used in this research project were capable of dispensing aliquots of ethylene gas with volumes close to but not exactly equal to those volumes listed in Table II. The data sets obtained from each experimental run were used to create spectra of the PA signal intensity (in mV) versus the rotational frequency of the mechanical chopper (in Hz).

Table II. Pre-determined volumes of ethylene gas needed to achieve desired concentrations of analyte gas

Cell #	Volume of Ethylene Gas Needed to Achieve Desired Concentrations of Analyte Gas (mL)				
	5%	10%	25%	50%	100%
1	4.77	9.53	23.8	47.7	95.3
2	17.09	34.18	85.45	170.9	341.8
3	32.45	64.90	162.3	324.5	649.0

As each aspect of the experimental setup was independently manipulated, the rotational frequency of the mechanical chopper was increased from 200 Hz to 4000 Hz in increments of 10 Hz. The data sets obtained from each experimental run were used to create spectra of the intensity of the PA signal (in mV) versus the rotational frequency (in Hz).

Each previously-obtained spectrum was evaluated to determine at what rotational frequencies relatively high PA signal intensities could be found. The exact values for the rotational frequencies that produced these peaks were determined by reanalyzing the PA signal intensities at and around these rotational frequencies. The exact values for the rotational frequencies were obtained by increasing the rotational frequency across a 20 Hz range at the approximate rotational frequencies that produced peaks prior. The rotational frequency of the mechanical chopper was increased in increments of 2 Hz. The range of rotational frequencies being reevaluated was increased as needed until a peak-like graph was obtained. In cases where a peak occurred at two or more consecutive or nearly-consecutive rotational frequencies, the median of the corresponding rotational frequencies was used. It was assumed that PA signal intensity could only be measured if a sinusoidal wave function was observed on the oscilloscope, indicating that the PA phenomenon was being observed. An overview of the experimental runs performed can be found in Table III.

Table III. Overview of experimental runs performed requiring manipulation of experimental setup

Run	Cell [Internal Radius of Cavity Resonator (cm)]	Concentrations of Analyte Gas Contained Within Cavity Resonator (%) [Volume of Analyte Gas Needed to Achieve Desired Concentrations (mL)]	Rotational Frequency of Mechanical Chopper (Hz)	Power of Light Source (%) [Exact Power of Light Source (mW)]	Windows
	1 (0.953) 2 (1.91) 3 (2.54) 4 (unknown)	5 10 25 50 100	200 - 4000 250	100 (291.0)	(1st, 2nd) C: coated UC: uncoated
A	1 (0.953)	5 (4.77)	200 - 4000	100 (291.0)	(C, C)
B	1 (0.953)	10 (9.53)	200 - 4000	100 (291.0)	(C, C)
C	1 (0.953)	25 (23.8)	200 - 4000	100 (291.0)	(C, C)
D	1 (0.953)	50 (47.7)	200 - 4000	100 (291.0)	(C, C)
E	1 (0.953)	100 (95.3)	200 - 4000	100 (291.0)	(C, C)
F	2 (1.91)	5 (17.09)	200 - 4000	100 (291.0)	(C, C)
G	2 (1.91)	10 (34.18)	200 - 4000	100 (291.0)	(C, C)
H	2 (1.91)	25 (85.45)	200 - 4000	100 (291.0)	(C, C)
I	2 (1.91)	50 (170.9)	200 - 4000	100 (291.0)	(C, C)
J	2 (1.91)	100 (341.8)	200 - 4000	100 (291.0)	(C, C)
K	3 (2.54)	5 (32.45)	200 - 4000	100 (291.0)	(C, C)
L	3 (2.54)	10 (64.90)	200 - 4000	100 (291.0)	(C, C)
M	3 (2.54)	25 (162.3)	200 - 4000	100 (291.0)	(C, C)
N	3 (2.54)	50 (324.5)	200 - 4000	100 (291.0)	(C, C)
O	3 (2.54)	100 (649.0)	200 - 4000	100 (291.0)	(C, C)
AJ	1 (0.953)	100 (95.3)	250	0 - 100 (0 - 291.0)	(UC, UC)

3.2.3: Part 3: Detection limit experiment

In the third part of this research project, a detection limit experiment was performed using Cells 1, 2, and 3 to formulate a qualitative discussion about how manipulating the internal radius of the cavity resonator influenced the concentration threshold at which a PA signal could be detected. To perform this experiment, a series of calculation should have been performed to determine the volume of analyte gas that needed to be added to each cavity resonator in order to displace 0.5%, 0.05%, and 0.005% of the pre-existing gas in each cavity resonator. These volumes would have been determined by multiplying the internal volumes for Cells 1, 2, and 3 by 0.005, 0.0005, and 0.00005. The volumes of ethylene gas that should have been added to each of the three cavity resonators to achieve desired concentration of 0.5%, 0.05%, and 0.005% are listed in Table IV. The pre-determined volumes of ethylene gas that should have been added to achieve a desired concentration of 5% were also listed in Table IV for comparative purposes.

Table IV. Pre-determined volumes of ethylene gas that should have been used in detection limit experiment

Cell #	Volume of Ethylene Gas Needed to Achieve Desired Concentrations of Analyte Gas (mL)			
	0.005%	0.05%	0.5%	5%
1	0.00477	0.0477	0.477	4.77
2	0.01709	0.1709	1.709	17.09
3	0.03245	0.3245	3.245	32.45

By accident, a series of calculations were performed to determine the volumes of analyte gas that needed to be added to each cavity resonator in order to displace 0.5%, 0.05%, and 0.005% of the pre-existing gas in Cell 1, 0.9494%, 0.09494%, and 0.009494% of the pre-existing

gas in Cell 2, and 1.000%, 0.1000%, and 0.01000% of the pre-existing gas in Cell 3. The volumes of ethylene gas that were added to Cells 1, 2, and 3 to achieve the previously-mentioned desired concentrations were listed in Table V, VI, and VII, respectively. The predetermined volumes of ethylene gas that should have been added to achieve a desired concentration of 5% were also listed.

Table V. Pre-determined volumes of ethylene gas used in detection limit experiment for Cell 1

Cell #	Volume of Ethylene Gas Needed to Achieve Desired Concentrations of Analyte Gas (mL)			
	0.005%	0.05%	0.5%	5%
1	0.00477	0.0477	0.477	4.77

Table VI. Pre-determined volumes of ethylene gas used in detection limit experiment for Cell 2

Cell #	Volume of Ethylene Gas Needed to Achieve Desired Concentrations of Analyte Gas (mL)			
	0.009494%	0.09494%	0.9494%	5%
2	0.03245	0.3245	3.245	17.09

Table VII. Pre-determined volumes of ethylene gas used in detection limit experiment and Cell 3

Cell #	Volume of Ethylene Gas Needed to Achieve Desired Concentrations of Analyte Gas (mL)			
	0.01000%	0.1000%	1.000%	5%
3	0.06490	0.6490	6.490	32.45

The ethylene gas was serially diluted to obtain the relatively low volumes of analyte gas needed to achieve the desired concentrations needed for trace gas detection. For example, to

collect and dispense 0.00477 mL of ethylene gas, a 10 mL syringe was filled with 1 mL of ethylene gas and 9 mL of air to produce a 10 mL ethylene-air solution with a concentration of 0.1 mL ethylene gas per mL ethylene-air solution. After allowing the ethylene-air solution to equilibrate within the 10 mL syringe, 9 mL of the gas solution was dispensed, and the syringe was filled once more with 9 mL of air to produce a 10 mL ethylene-air solution with a concentration of 0.01 mL ethylene gas per mL ethylene-air solution. 4.77 ml of this ethylene-air solution was dispensed into Cell 1 to achieve a desired concentration of 0.005%. This procedure was repeated for Cells 1, 2, and 3 to achieve the gas concentrations needed for use in the detection limit experiment.

The data sets obtained in the second part of this research project were used to help generate some of the spectra necessary for this part of the research project. In particular, the data sets obtained upon reevaluation of the peaks generated in Runs A, F, and K were used to determine the range of rotational frequencies that needed to be analyzed for determination of the detection limit for each cavity resonator. Based on the data obtained in the second part of this experiment, the exact rotational frequencies that produced peaks with the greatest amplitudes when Cells 1, 2, and 3 contained 5% ethylene gas by volume were determined to be 292 Hz, 510 Hz, and 237 Hz, respectively. The rotational frequency was scanned across a 12 Hz range around 292 Hz in increments of 2 Hz to determine the intensities of the PA signal when Cell 1 contained 0.50%, 0.05%, and 0.005% ethylene gas by volume. This process was performed twice more using 510 Hz and 237 Hz (versus 292 Hz) for Cells 2 and 3, respectively. Each data set obtained was used to create a spectrum of the intensity of the PA signal (in mV) versus the rotational frequency (in Hz).

Chapter 4: Results and Analysis

Table of Contents

4.1: Infrared spectra of ethylene and nitrogen

The IR spectrum of ethylene gas can be found in Figure VI. The absorption wavelength of ethylene gas was experimentally determined to exist around the wavelength 10.6 μm.

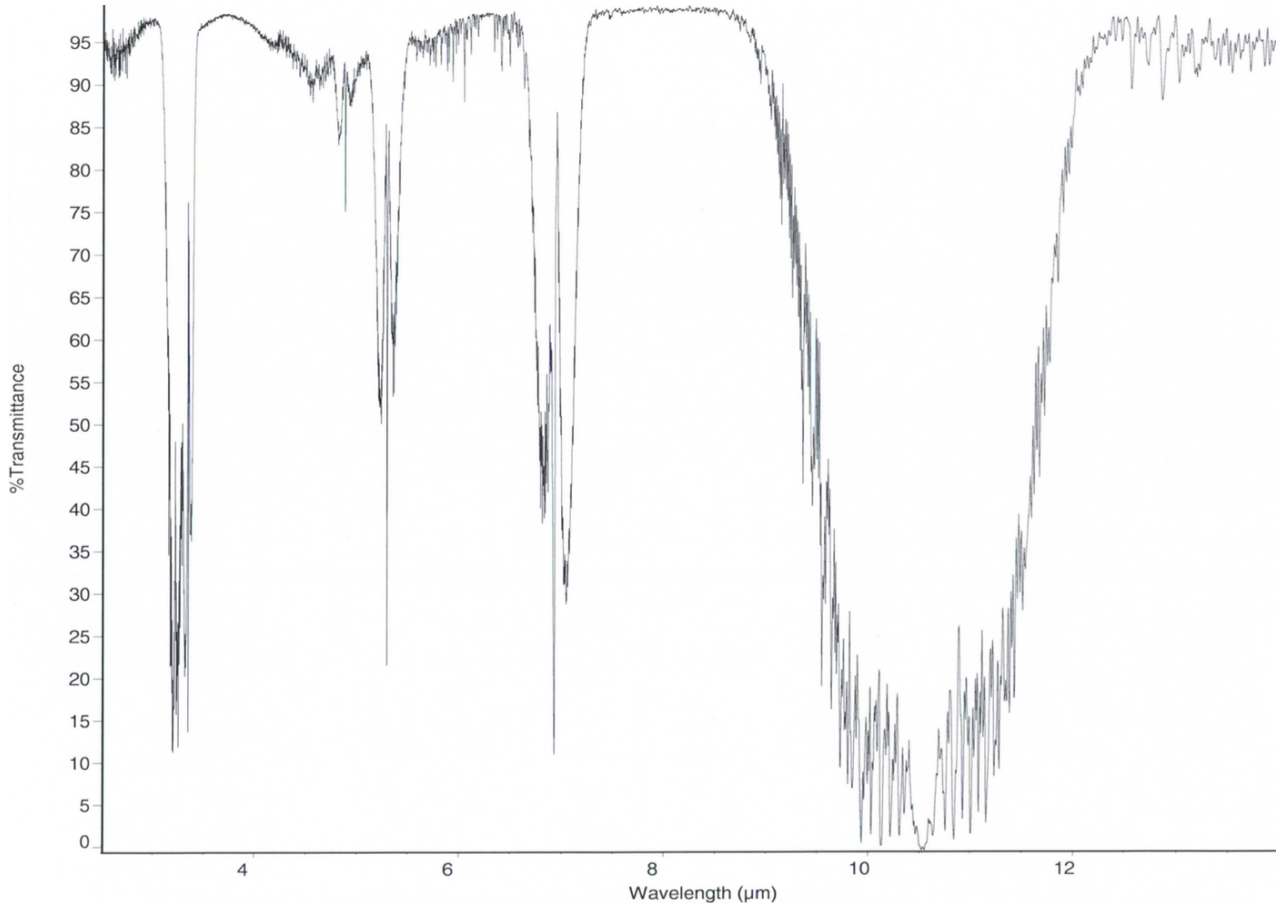

Figure VI. Infrared spectrum of ethylene gas

The IR spectrum of nitrogen gas can be found in Figure VII. The IR spectrum revealed an absorption wavelength that was located neither at or around the wavelength 10.6 μm.

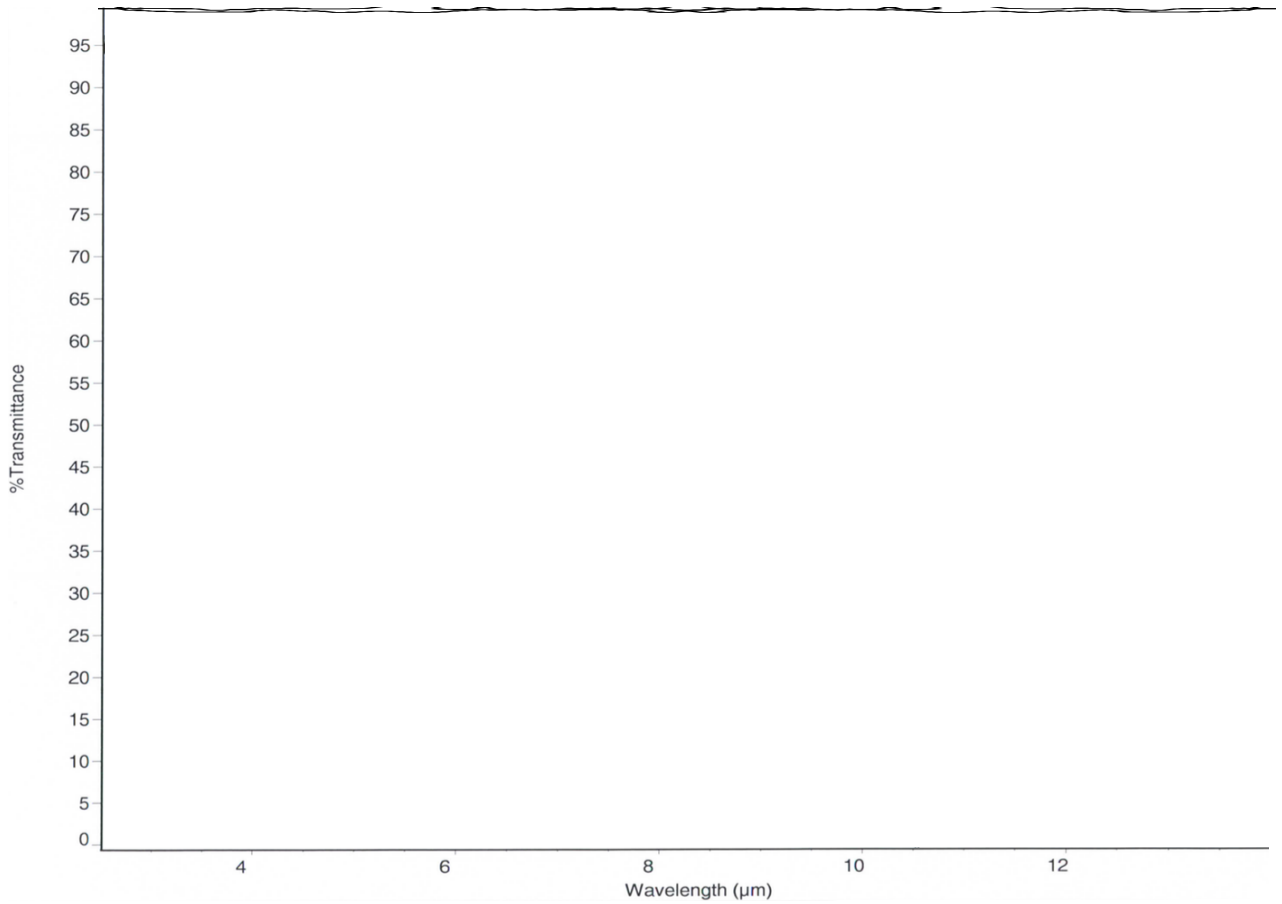

Figure VII. Infrared spectrum of nitrogen gas

4.2: Experimental runs with manipulated parameters

A summary of the experimental runs performed in this part of the research project can be found in Table III. The data sets obtained from Runs A - O were used to create spectra of the intensity of the PA signal (in mV) versus the rotational frequency (in Hz). Each peak observed in each of the aforementioned spectra was reevaluated to determine the exact values for the rotational frequencies that produced these peaks. Hereafter, Run A2 refers to the data set obtained upon reevaluation of the spectra generated from Run A, Run B2 refers to the data set obtained upon reevaluation of the spectra generated from Run B, Run C2 refers to the data set obtained upon reevaluation of the spectra generated from Run C, and so forth. The data sets obtained from Runs A2 - O2 were also used to create spectra of the intensity of the PA signal (in mV) versus the rotational frequency (in Hz) but only in cases where a sinusoidal wave function was observed on the oscilloscope. The spectra for Runs A2 - O2 can also be found below. Not all peaks observed upon initial evaluation of the spectra for Runs A - O were re-observed upon evaluation of the spectra for Runs A2 - O2; therefore, to help maintain the integrity of the data sets gathered in this research project that will later be used to help formulate a discussion about the PA effect of ethylene, the spectra for Runs A - O can also be found below.

The spectra for Runs A - E were superimposed to help visualize how the intensity of the PA signal changed as the concentration of analyte gas contained within Cell 1 was manipulated. Note that the internal radius of the cavity resonator was held constant for Runs A - E. The resulting spectrum can be found below in Figure VIII. For Run A, peaks were observed at rotational frequencies of approximately 290 Hz, 560 Hz, 680 Hz, 1130 Hz, 1535 Hz, 1860 Hz, and 2155 Hz. For Run B, peaks were observed at rotational frequencies of approximately 290 Hz, 680 Hz, 1130 Hz, 1540 Hz, and 1860 Hz. For Run C, peaks were observed at rotational frequencies of

approximately 290 Hz, 680 Hz, 1120 Hz, 1530 Hz, 1860 Hz, 2260 Hz, and 2705 Hz. For Run D, peaks were observed at rotational frequencies of approximately 290 Hz, 670 Hz, 1110 Hz, 1510 Hz, 1850 Hz, 1930 Hz, 2235 Hz, and 2680 Hz. Finally, for Run E, peaks were observed at rotational frequencies of approximately 280 Hz, 650 Hz, 1070 Hz, 1460 Hz, 1770 Hz, 2160 Hz, 2590 Hz, 3000 Hz, 3590 Hz, and 3930 Hz.

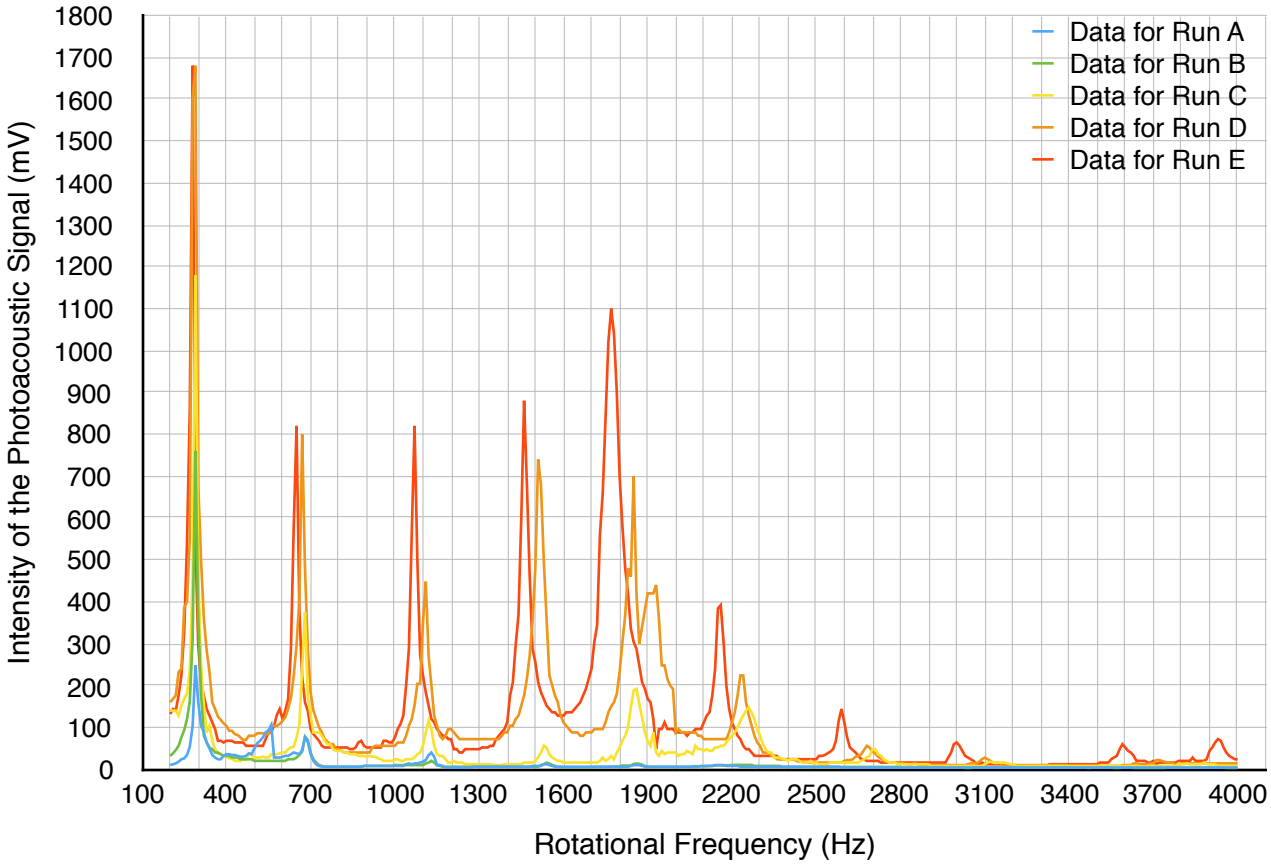

Figure VIII. Superimposed spectra for Runs A - E

The spectra for Runs A2 - E2 were superimposed. The resulting spectrum can be found below in Figure IX. For Run A2, peaks were observed at rotational frequencies of 292 Hz, 558 Hz, 679 Hz, 1121 Hz, 1531 Hz, 1863 Hz and 2151 Hz. For Run B2, peaks were observed at rotational frequencies of 290 Hz, 676 Hz, 1120 Hz, 1531 Hz, and 1864 Hz. For Run C2, peaks were observed at rotational frequencies of 288 Hz, 674 Hz, 1110 Hz, 1523 Hz, 1853 Hz, and 2245 Hz. For Run D2, peaks were observed at rotational frequencies of 286 Hz, 667 Hz, 1100 Hz, 1506 Hz, 1830 Hz, and 2220 Hz. Finally, for Run E2, peaks were observed at rotational frequencies of 278 Hz, 650 Hz, 1074 Hz, 1468 Hz, 1778 Hz, 2160 Hz, 2592 Hz, 2996 Hz, and 3590 Hz.

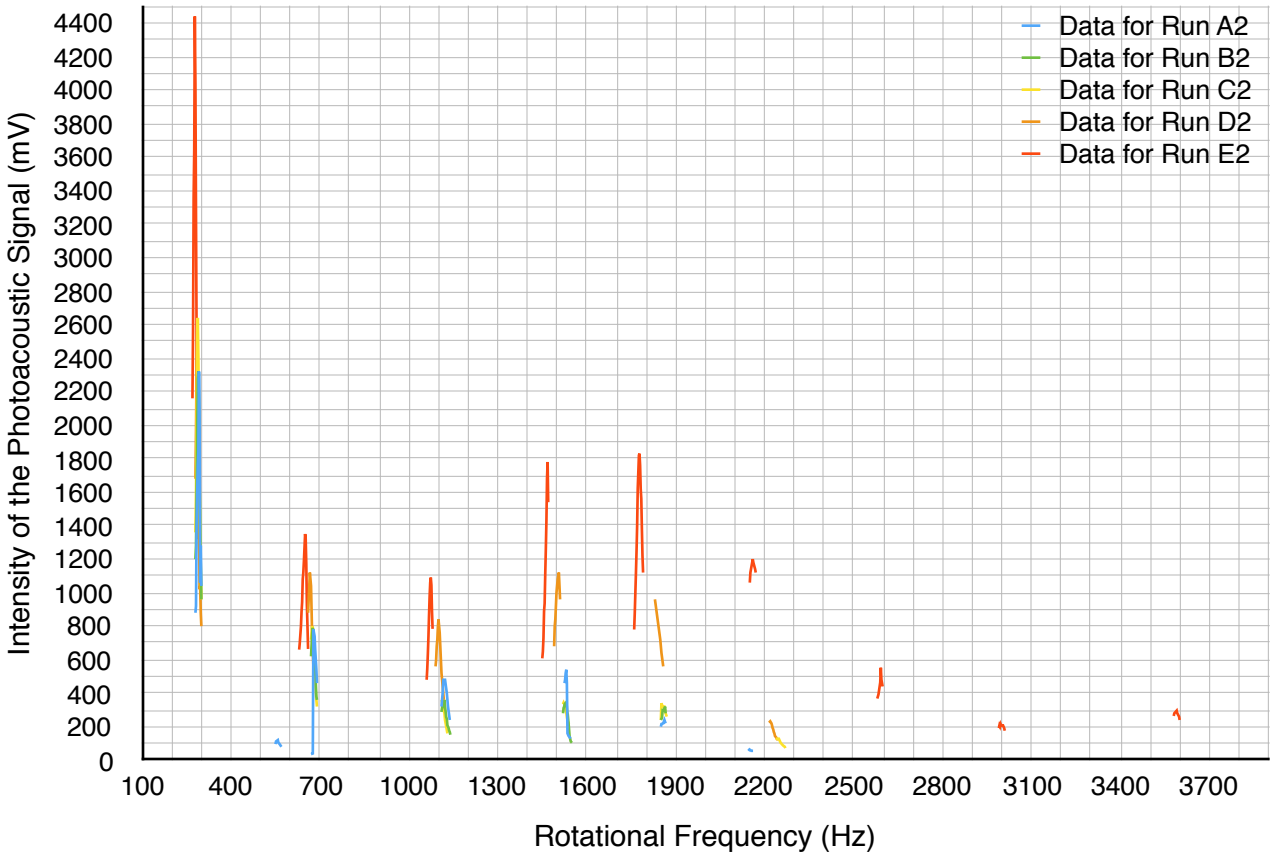

Figure IX. Superimposed spectra for Runs A2 - E2

The spectra for Runs F - J were superimposed to help visualize how the intensity of the PA signal changed as the concentration of analyte gas contained within Cell 2 was manipulated. Note that the internal radius of the cavity resonator was held constant for Runs F - J. The resulting spectrum can be found below in Figure X. For Run F, peaks were observed at rotational frequencies of approximately 310 Hz, 510 Hz, 710 Hz, and 1320 Hz. For Run G, peaks were observed at rotational frequencies of approximately 300 Hz, 510 Hz, 720 Hz, and 2470 Hz. For Run H, peaks were observed at rotational frequencies of approximately 325 Hz, 510 Hz, 720 Hz, 1920 Hz, and 2500 Hz. For Run I, peaks were observed at rotational frequencies of approximately 380 Hz, 500 Hz, 710 Hz, 1910 Hz, 2450 Hz, and 2760 Hz. Finally, for Run J, peaks were observed at rotational frequencies of approximately 380 Hz, 490 Hz, 680 Hz, 2340 Hz, 2625 Hz and 3840 Hz.

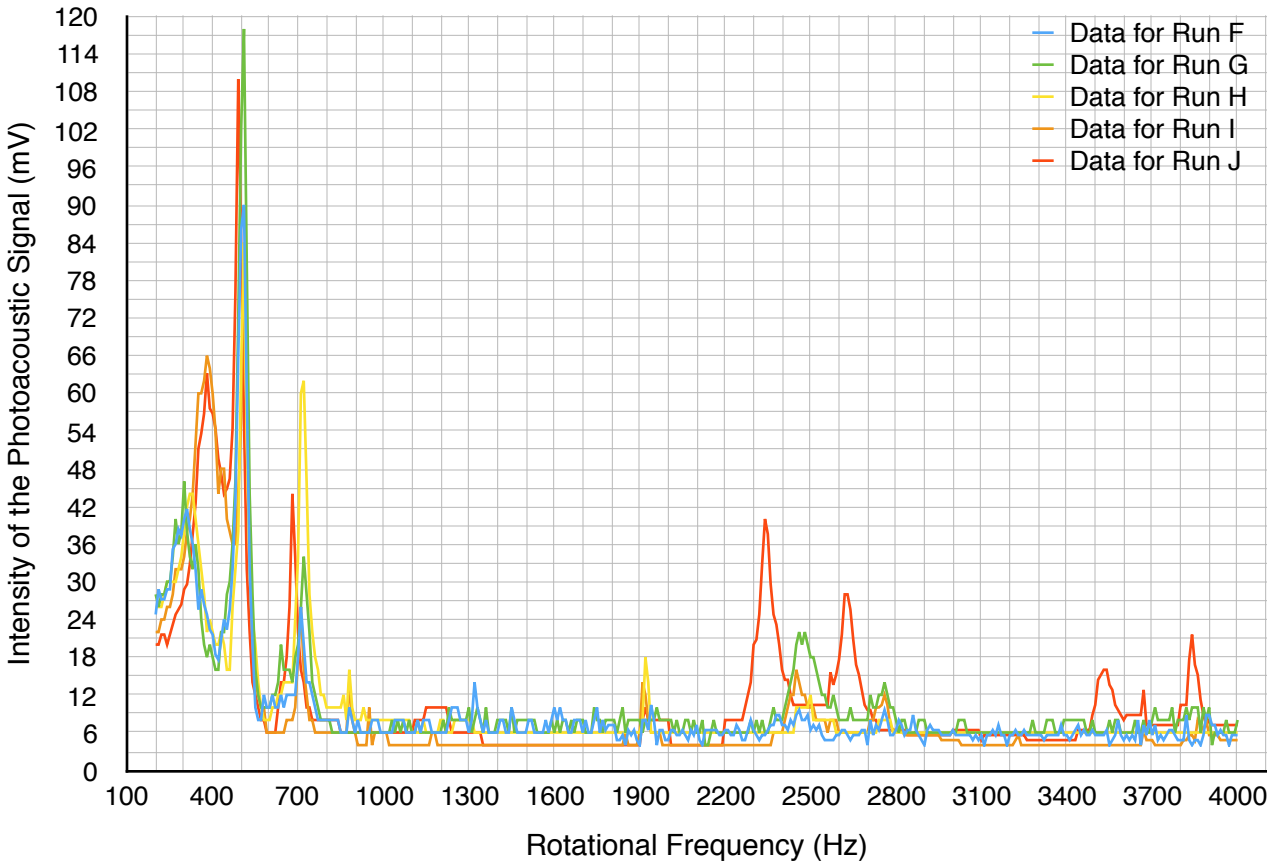

Figure X. Superimposed spectra for Runs F - J

The spectra for Runs F2 - J2 were superimposed. The resulting spectrum can be found below in Figure XI. For Run F2, a peak was observed at a rotational frequency of 510 Hz. For Run G2, no peaks were observed. For Run H2, peaks were observed at rotational frequencies of 341 Hz, 508 Hz, and 708 Hz. For Run I2, peaks were observed at rotational frequencies of 384 Hz, 506 Hz, and 700 Hz. Finally, for Run J2, peaks were observed at rotational frequencies of 400 Hz, 504 Hz, and 701 Hz.

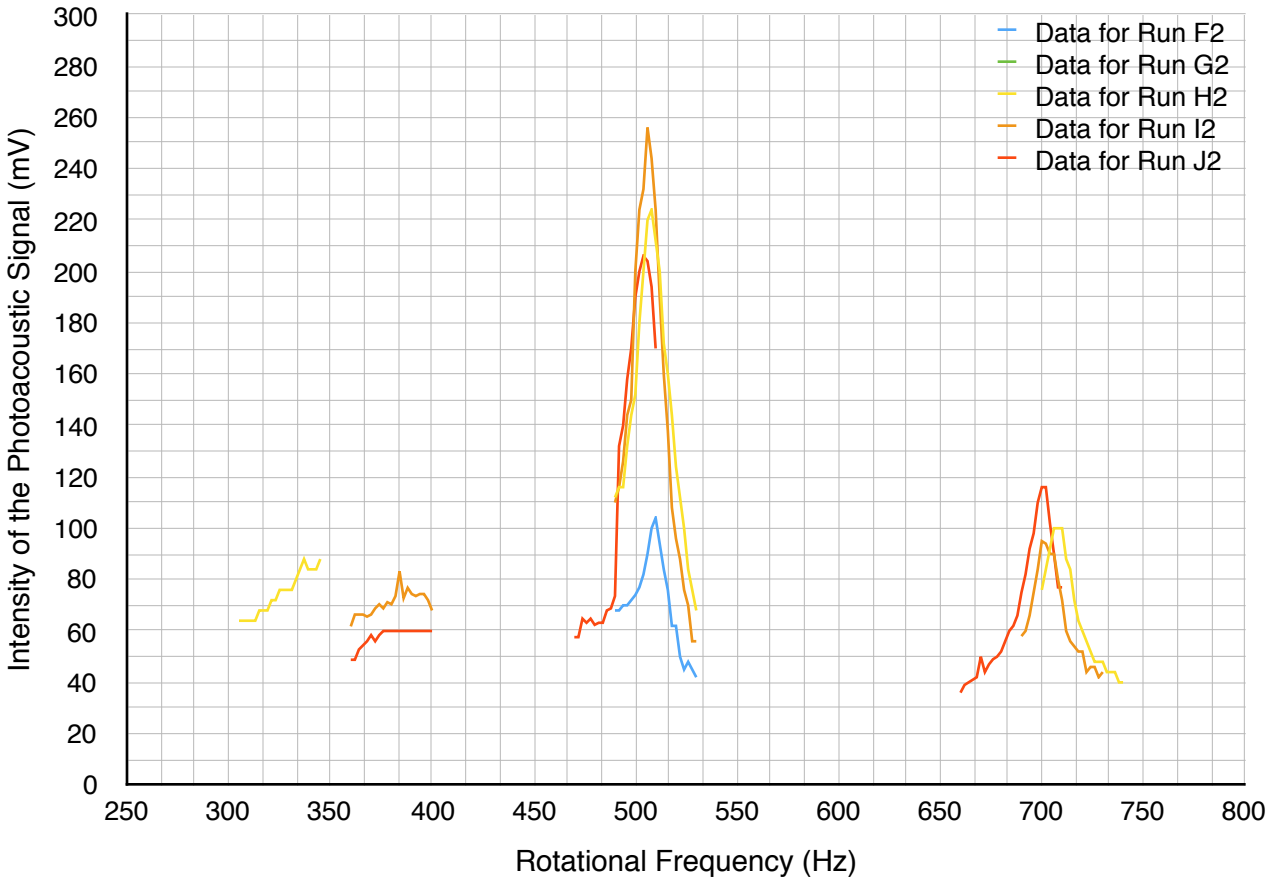

Figure XI. Superimposed spectra for Runs F2 - J2

The spectra for Runs K - O were superimposed to help visualize how the intensity of the PA signal changed as the concentration of analyte gas contained within Cell 3 was manipulated. Note that the internal radius of the cavity resonator was held constant for Runs K - O. The resulting spectrum can be found below in Figure XII. For Run K, peaks were observed at rotational frequencies of approximately 240 Hz and 740 Hz. For Run L, peaks were observed at rotational frequencies of approximately 230 Hz, 300 Hz, 500 Hz, and 750 Hz. For Run M, peaks were observed at rotational frequencies of approximately 230 Hz, 500 Hz, 740 Hz, 2060 Hz, and 2350 Hz. For Run N, peaks were observed at rotational frequencies of approximately 200 Hz, 2030 Hz, 2310 Hz, and 2785 Hz. Finally, for Run O, peaks were observed at rotational frequencies of approximately 670 Hz and 2030 Hz.

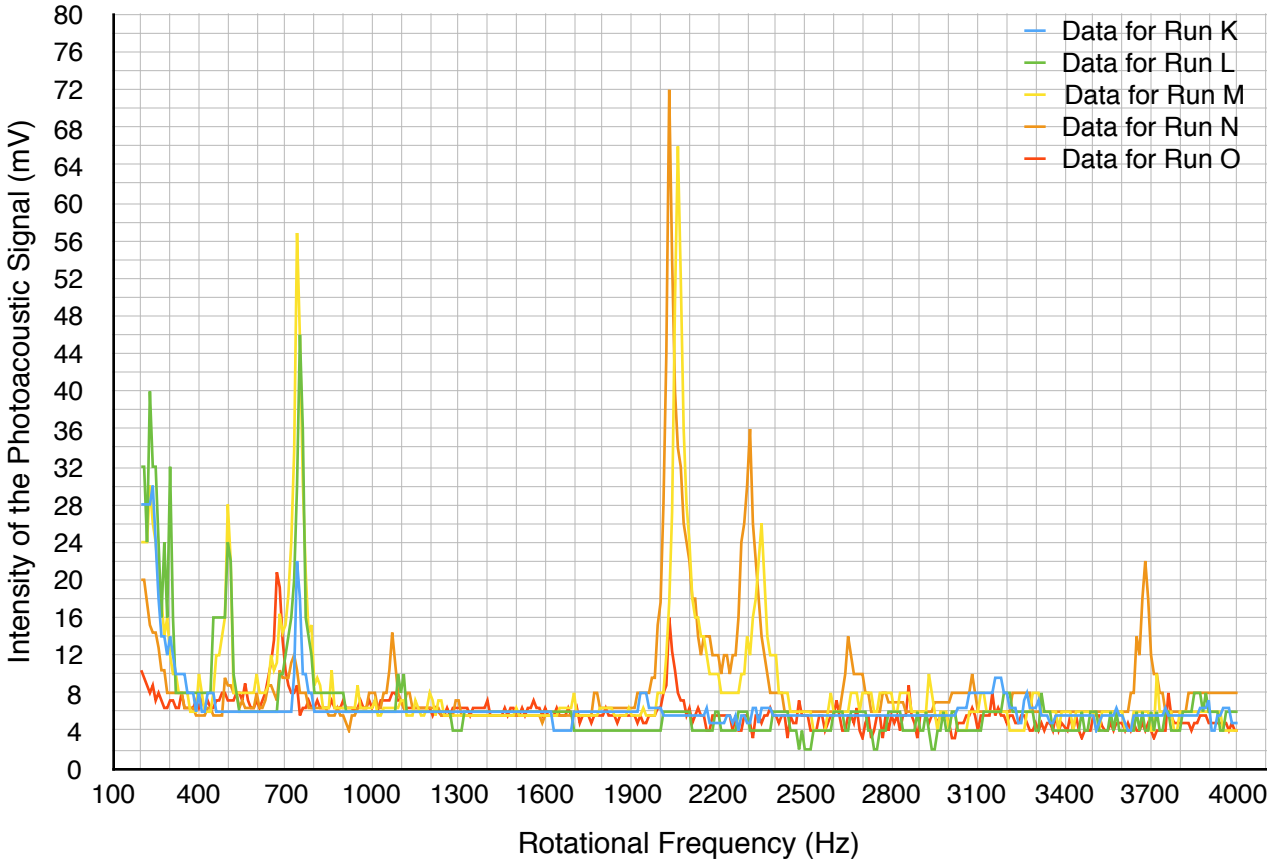

Figure XII. Superimposed spectra for Runs K - O

The spectra for Runs K2 - O2 were superimposed. The resulting spectrum can be found below in Figure XIII. For Run K2, a peak was observed at a rotational frequency of 237 Hz. For Run L2, peaks were observed at rotational frequencies of 210 Hz and 301 Hz. For Run M2, a peak was observed at a rotational frequency of 2342 Hz. For Run N2, peaks were observed at rotational frequencies of 218 Hz and 2020 Hz. Finally, for Run O2, no peaks were observed.

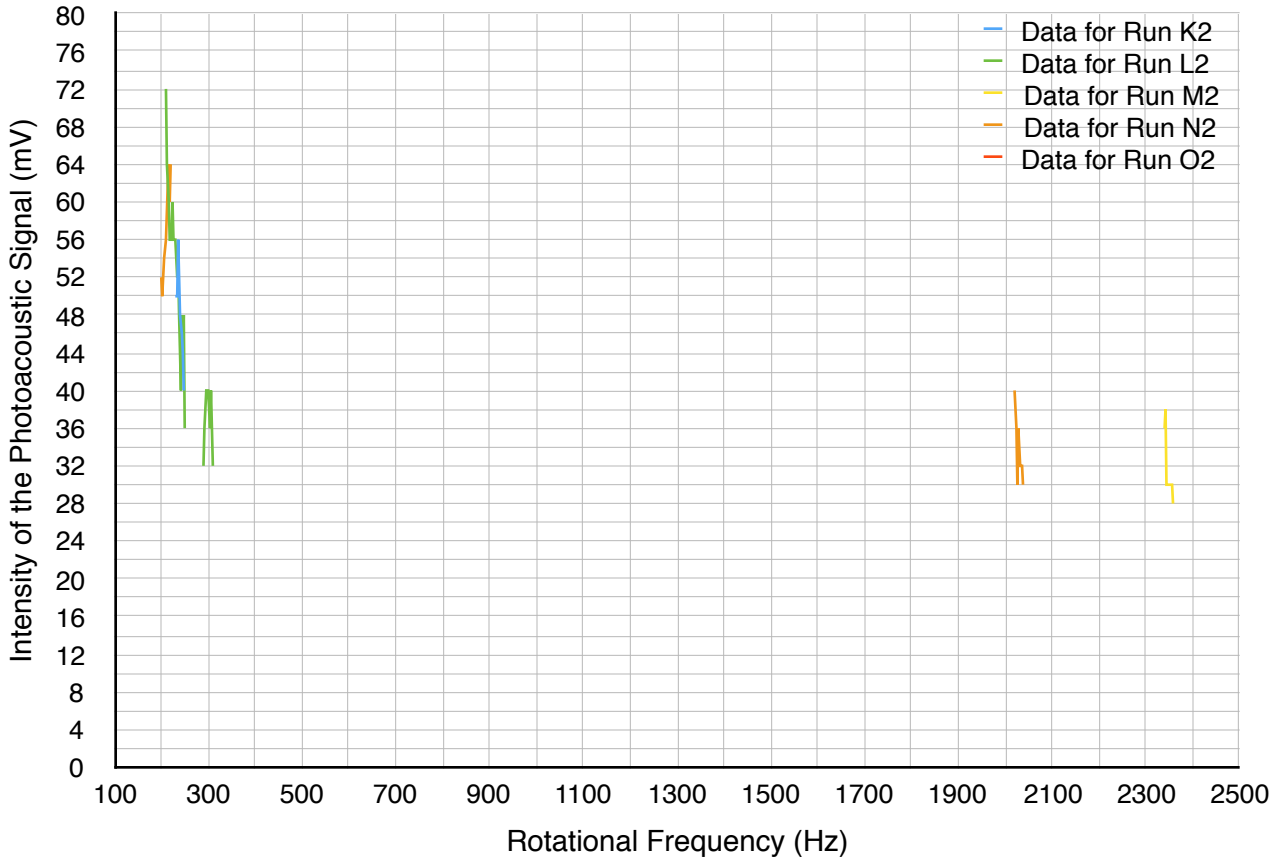

Figure XIII. Superimposed spectra for Runs K2 - O2

The spectra for Runs A, F, and K were superimposed to help visualize how the intensity of the PA signal changed when the internal radius of the cavity resonator was manipulated but the concentration of analyte gas contained within each cavity resonator was held constant at 5%. The resulting spectrum can be found below in Figure XIV.

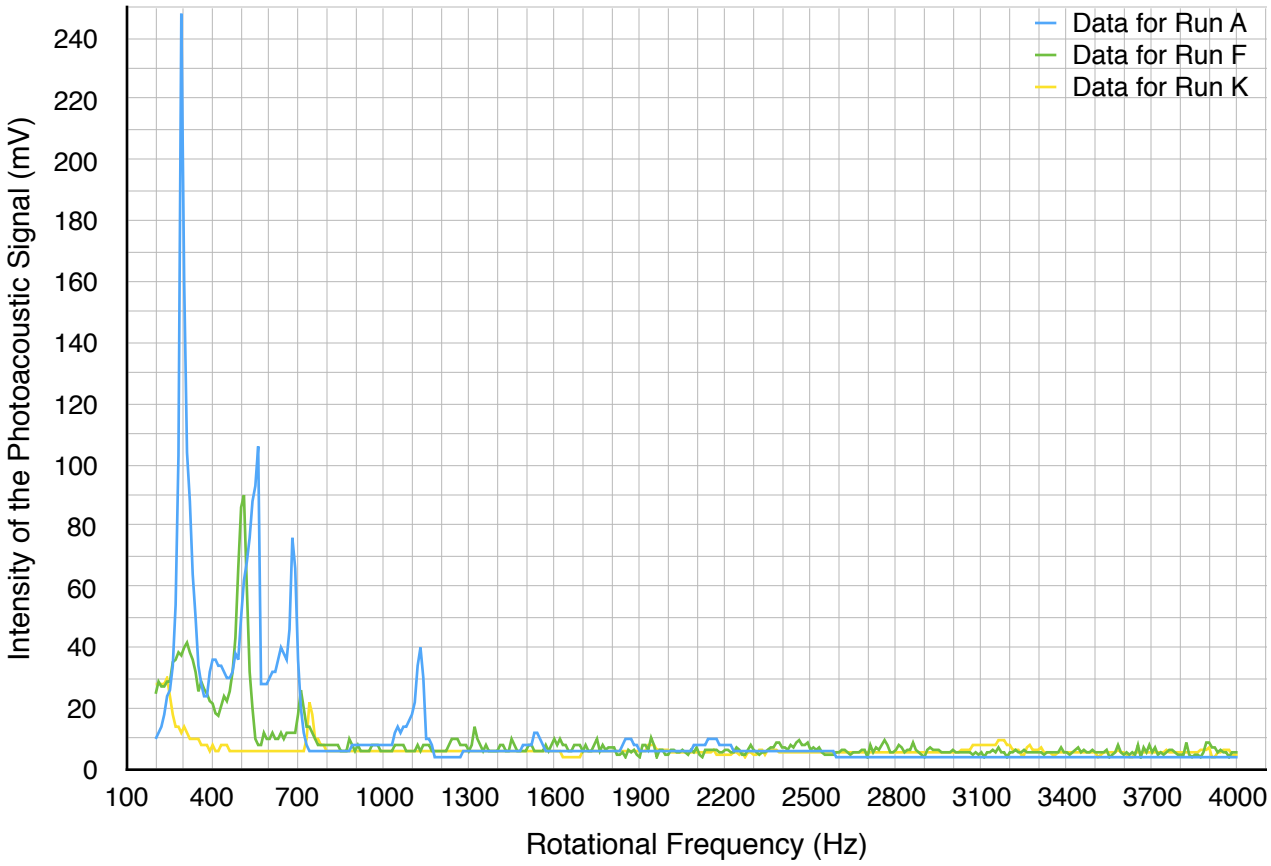

Figure XIV. Superimposed spectra for Runs A, F, K

The spectra for Runs A2, F2, and K2 were superimposed. The resulting spectrum can be found below in Figure XV.

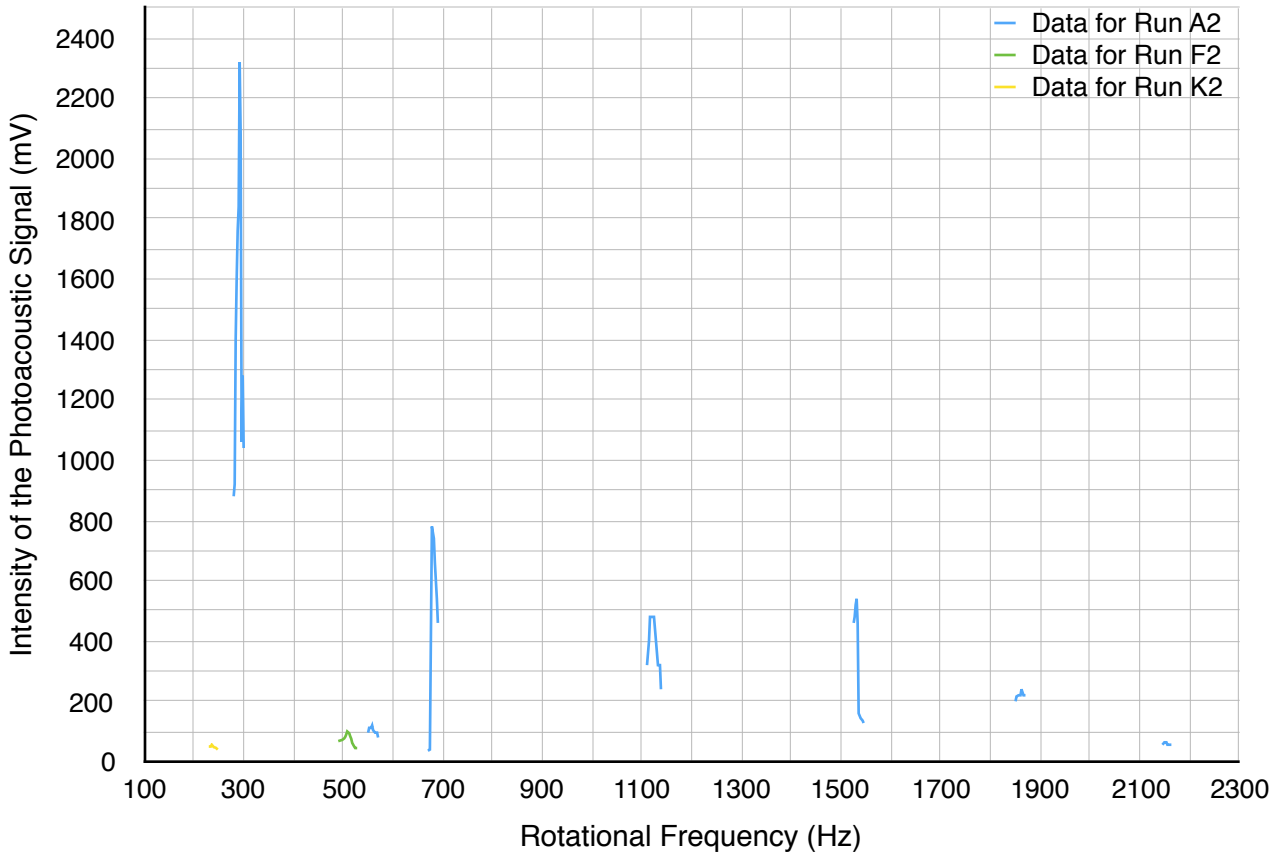

Figure XV. Superimposed spectra for Runs A2, F2, K2

The spectra for Runs B, G, and L were superimposed to help visualize how the intensity of the PA signal changed when the internal radius of the cavity resonator was manipulated but the concentration of analyte gas contained within each cavity resonator was held constant at 10%. The resulting spectrum can be found below in Figure XVI.

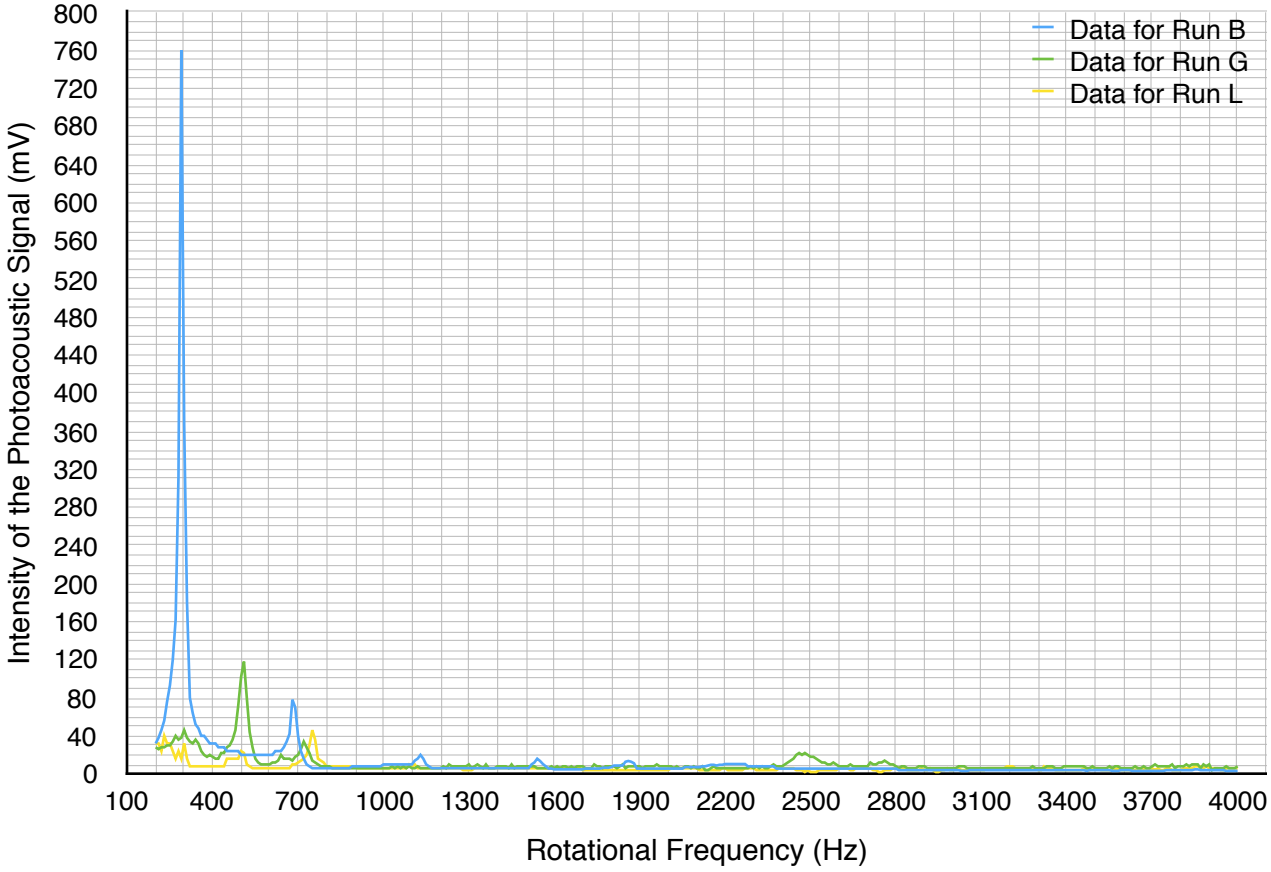

Figure XVI. Superimposed spectra for Runs B, G, L

The spectra for Runs B2, G2, and L2 were superimposed. The resulting spectrum can be found below in Figure XVII.

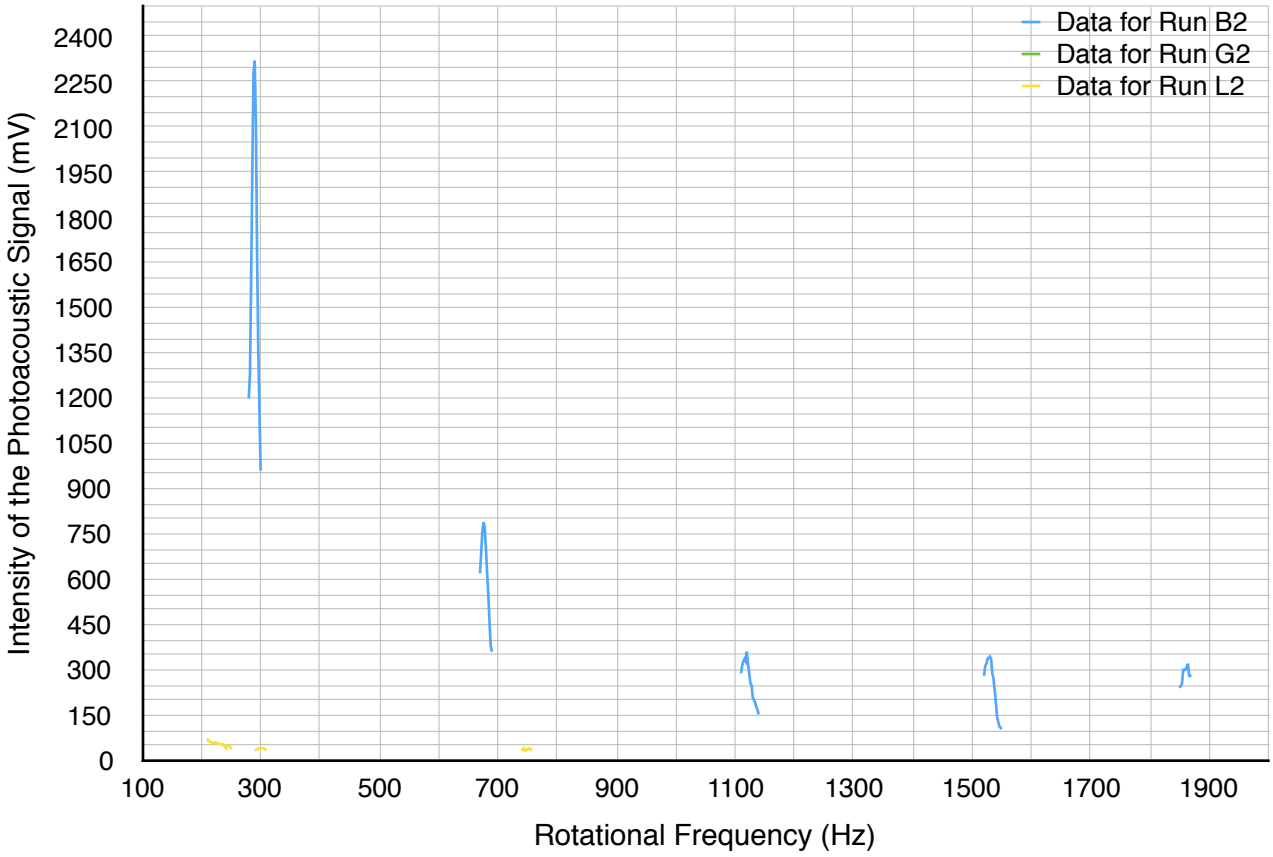

Figure XVII. Superimposed spectra for Runs B2, G2, L2

The spectra for Runs C, H, and M were superimposed to help visualize how the intensity of the PA signal changed when the internal radius of the cavity resonator was manipulated but the concentration of analyte gas contained within each cavity resonator was held constant at 25%. The resulting spectrum can be found below in Figure XVIII.

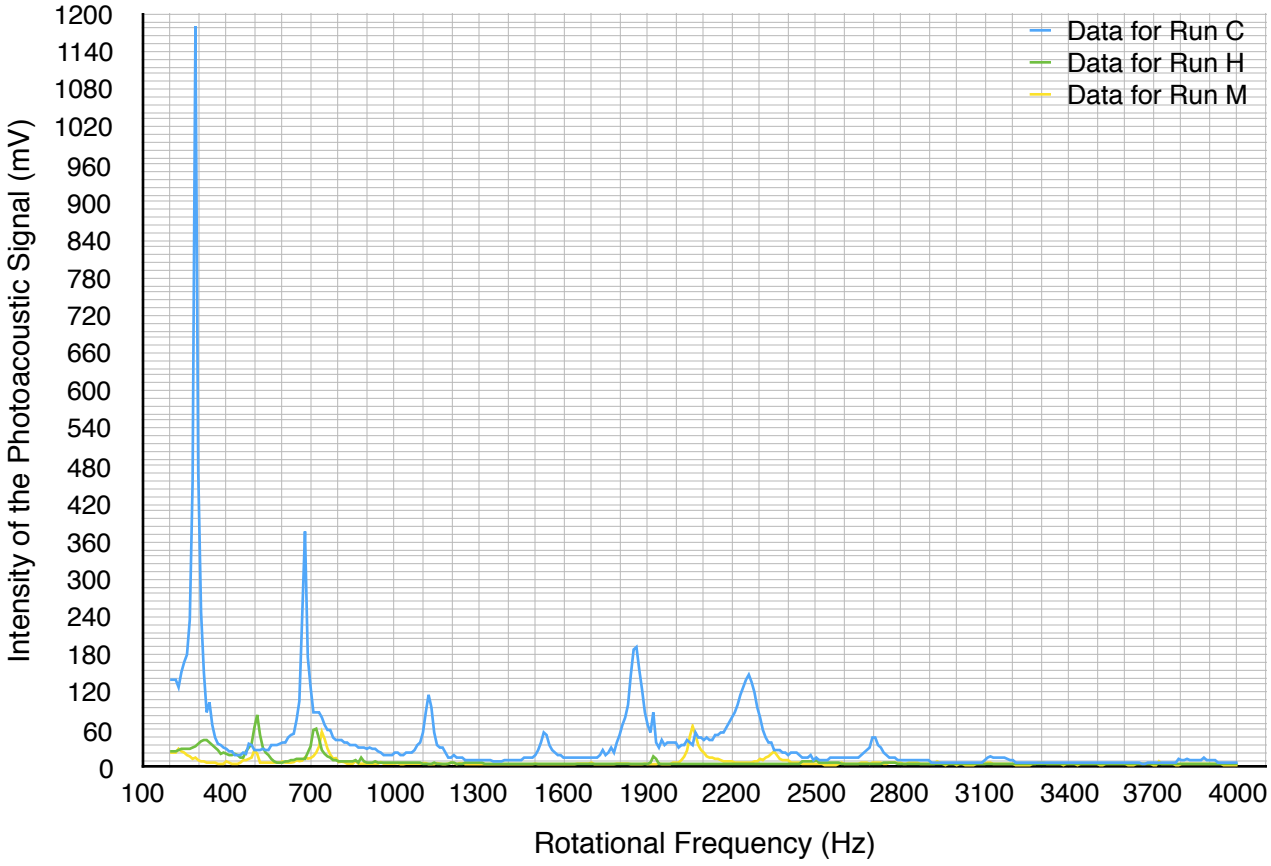

Figure XVIII. Superimposed spectra for Runs C, H, M

The spectra for Runs C2, H2, and M2 were superimposed. The resulting spectrum can be found below in Figure XIX.

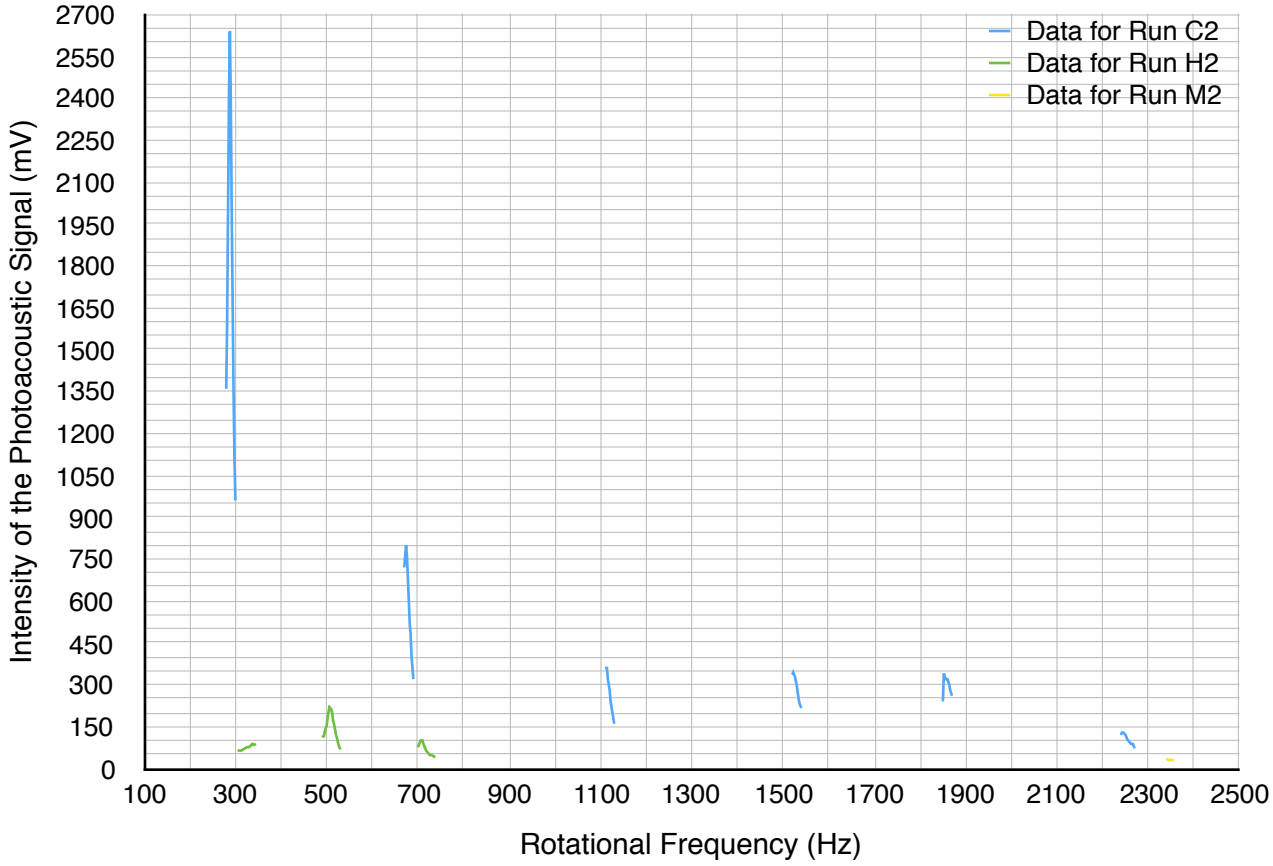

Figure XIX. Superimposed spectra for Runs C2, H2, M2

The spectra for Runs D, I, and N were superimposed to help visualize how the intensity of the PA signal changed when the internal radius of the cavity resonator was manipulated but the concentration of analyte gas contained within each cavity resonator was held constant at 50%. The resulting spectrum can be found below in Figure XX.

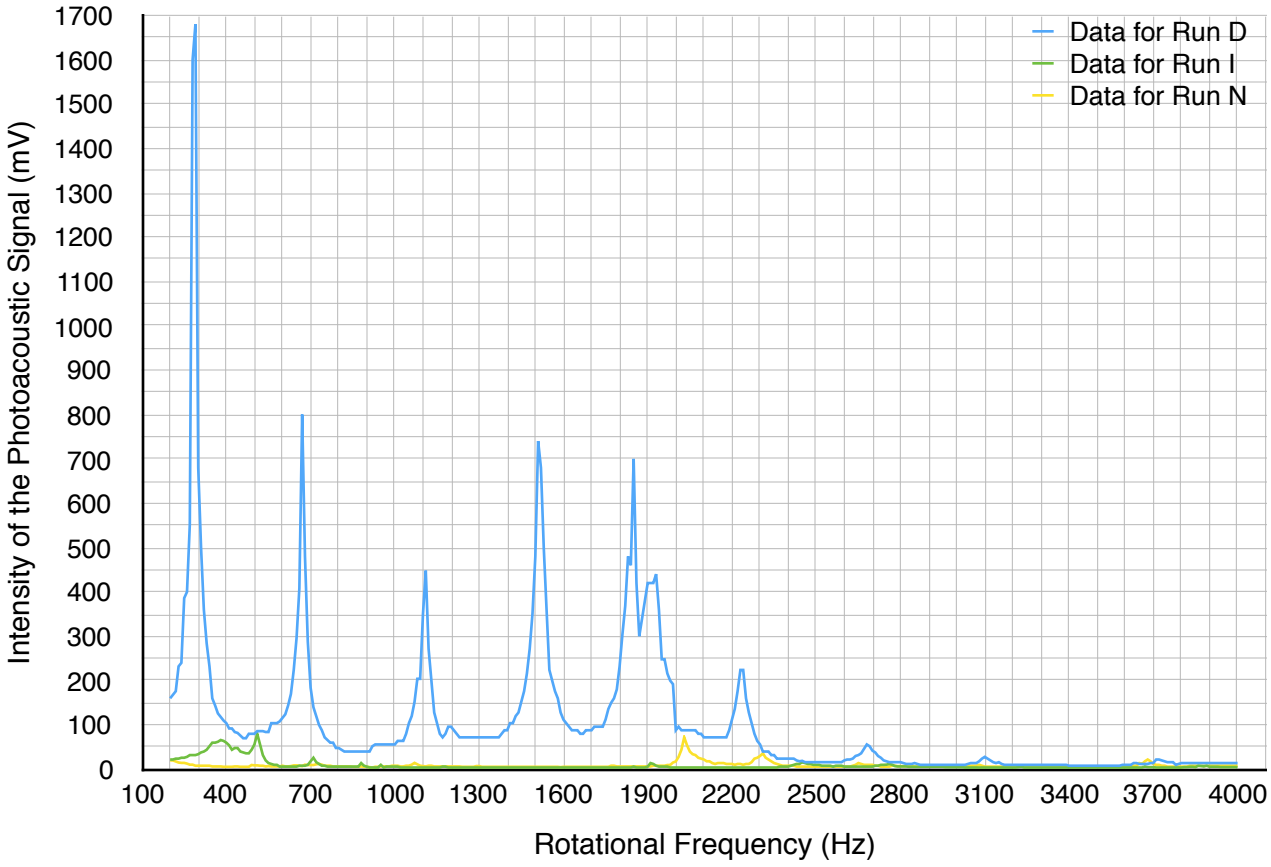

Figure XX. Superimposed spectra for Runs D, I, N

The spectra for Runs D2, I2, and N2 were superimposed. The resulting spectrum can be found below in Figure XXI.

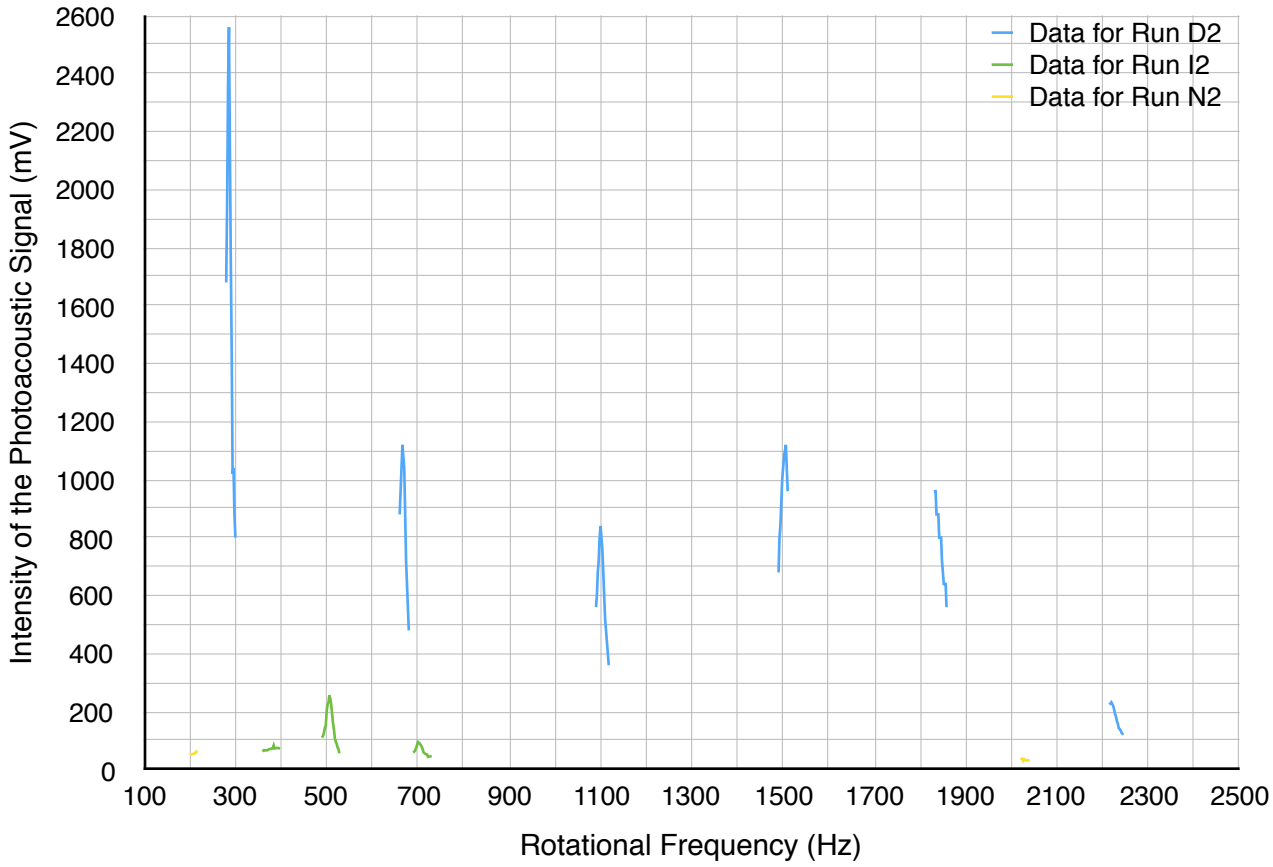

Figure XXI. Superimposed spectra for Runs D2, I2, N2

The spectra for Runs E, J, and O were superimposed to help visualize how the intensity of the PA signal changed when the internal radius of the cavity resonator was manipulated but the concentration of analyte gas contained within each cavity resonator was held constant at 100%. The resulting spectrum can be found below in Figure XXII.

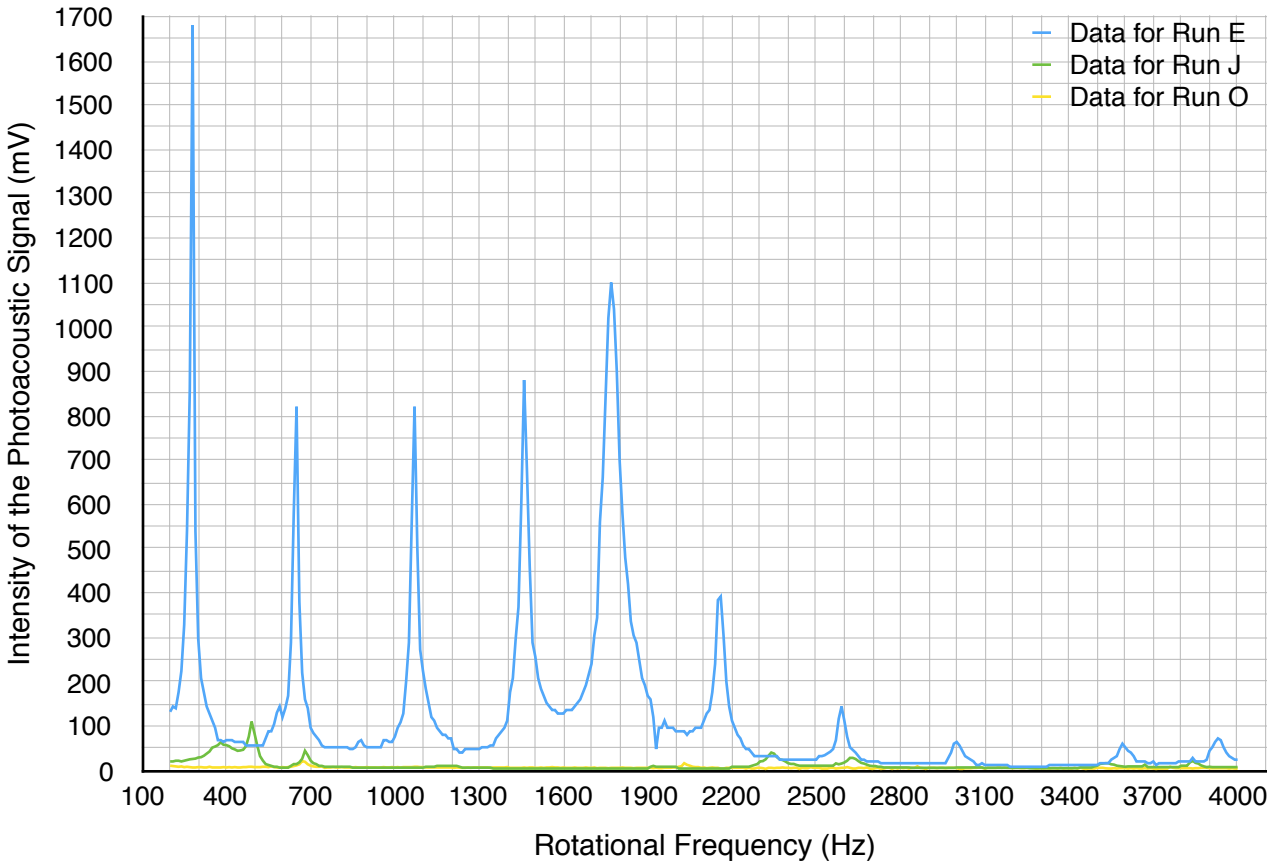

Figure XXII. Superimposed spectra for Runs E, J, O

The spectra for Runs E2, J2, and O2 were superimposed. The resulting spectrum can be found below in Figure XXIII.

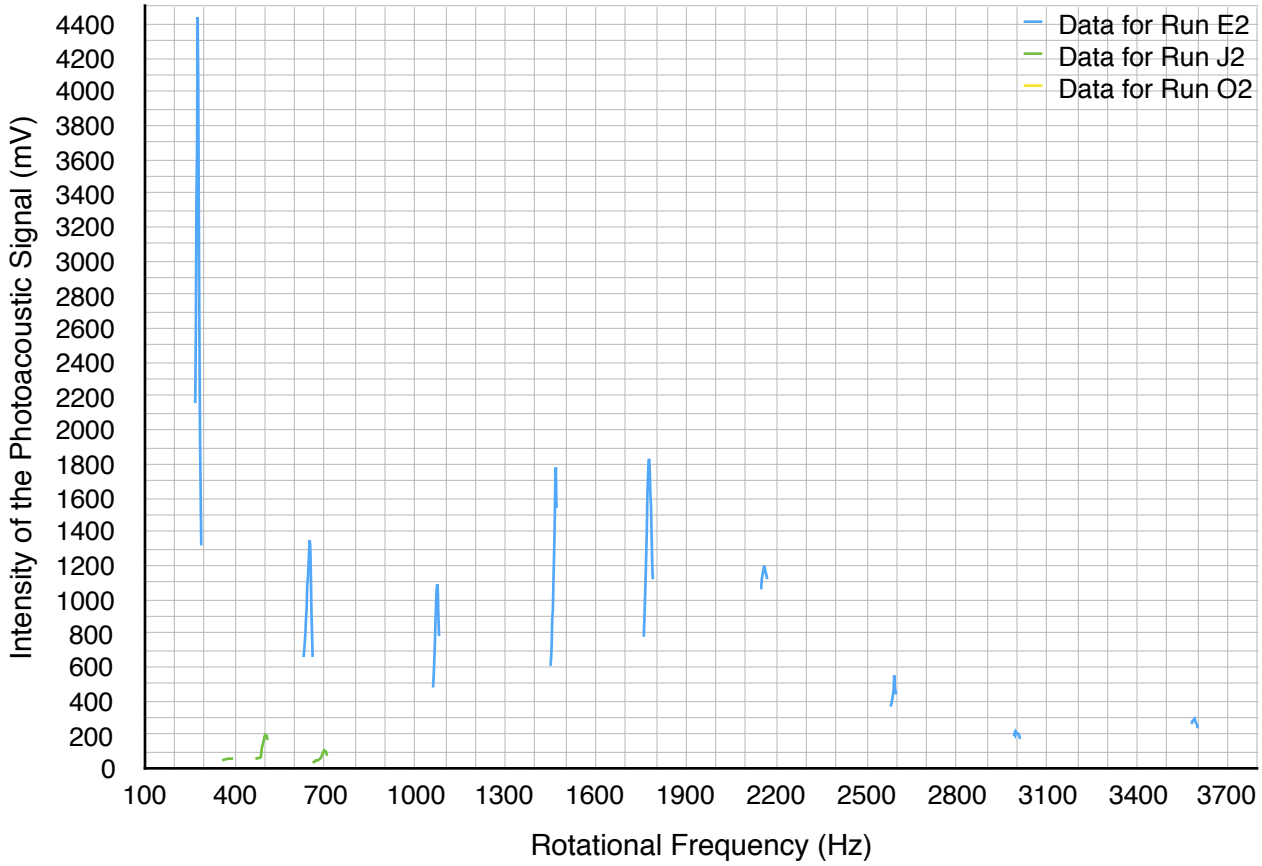

Figure XXIII. Superimposed spectra for Runs E2, J2, O2

The adjusted values for the intensity of the PA signal (and the unadjusted values for the intensity of the PA signal) as a function of increasing laser power are listed below in Table XIII and plotted in Figure XXIV.

Table XIII. Intensity of the photoacoustic signal as a function of increasing laser power

Laser Power (mW)	Unadjusted Intensity of the Photoacoustic Signal (mV)	Adjusted Intensity of the Photoacoustic Signal (mV)
0	56	0
2	64	8
26	83	27
53	97	41
60	104	48
81	110	54
120	153	97
140	168	112

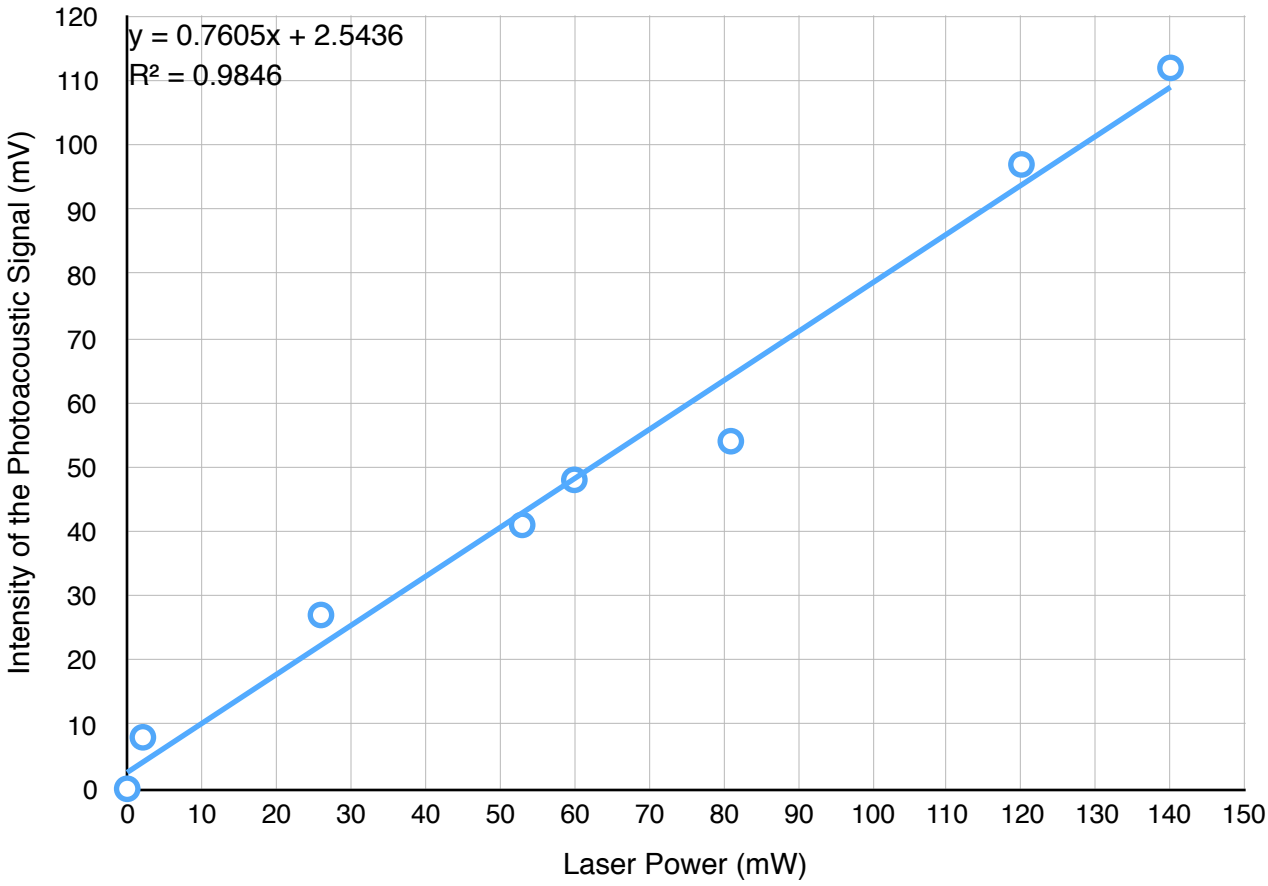

Figure XXIV. Intensity of the photoacoustic signal as a function of increasing laser power

4.3: Detection limit experiment

The volumes of ethylene gas needed to achieve desired concentrations of 5%, 0.5%, 0.05%, and 0.005% for Cell 1, 5%, 0.9494%, 0.09494%, and 0.009494% for Cell 2, and 5%, 1%, 0.1%, and 0.01% for Cell 3 are listed in Tables V, VI, and VII, respectively. The data sets obtained were used to create spectra of the intensity of the PA signal (in mV) versus the rotational frequency (in Hz). The four spectra generated for Cell 1 in this part of the research project were superimposed to help visualize how the intensity of the PA signal changed when the concentration of ethylene gas contained within Cell 1 was manipulated. Note that the internal radius of the cavity resonator was held constant. The resulting spectra can be found in Figures XXV and XXVI.

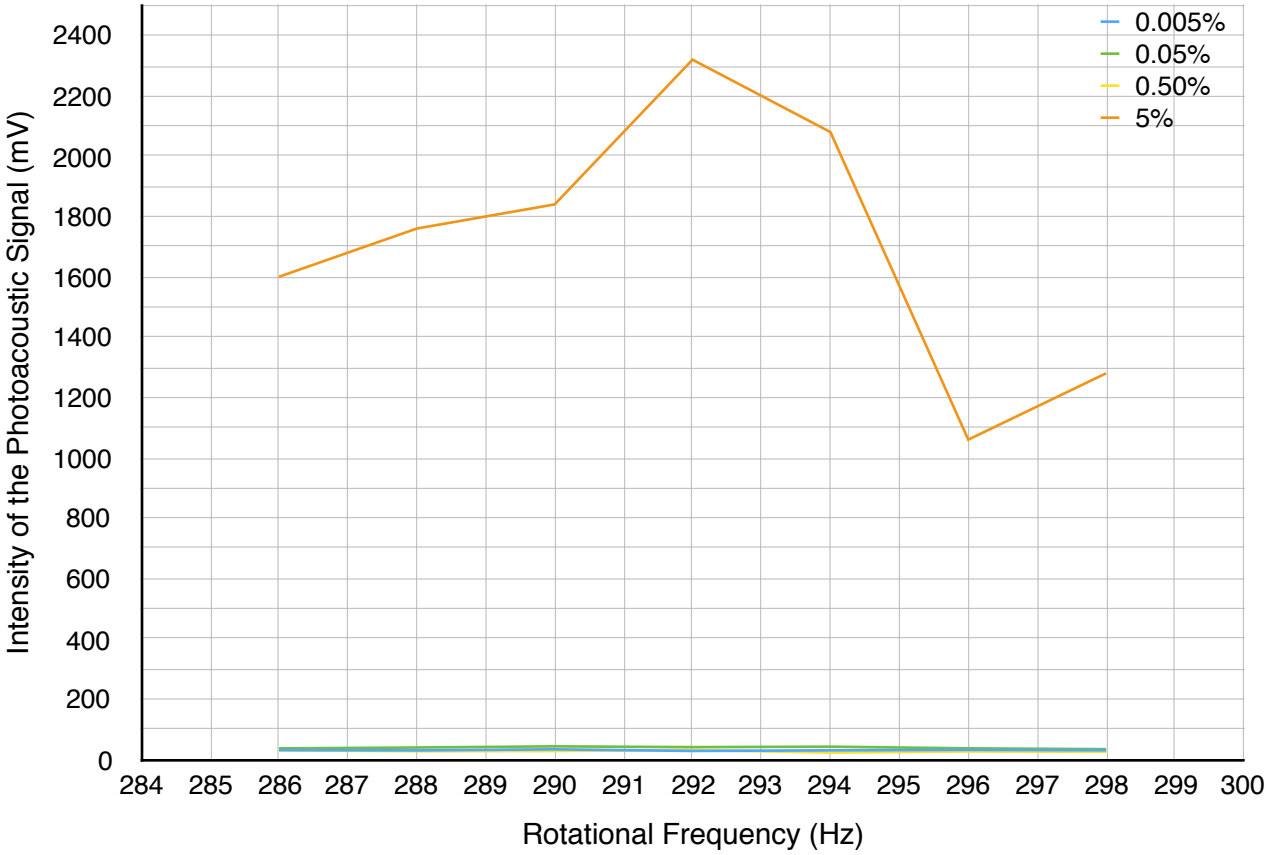

Figure XXV. Superimposed spectra of 5%, 0.5%, 0.05%, and 0.005% concentration ethylene gas in Cell 1 by volume

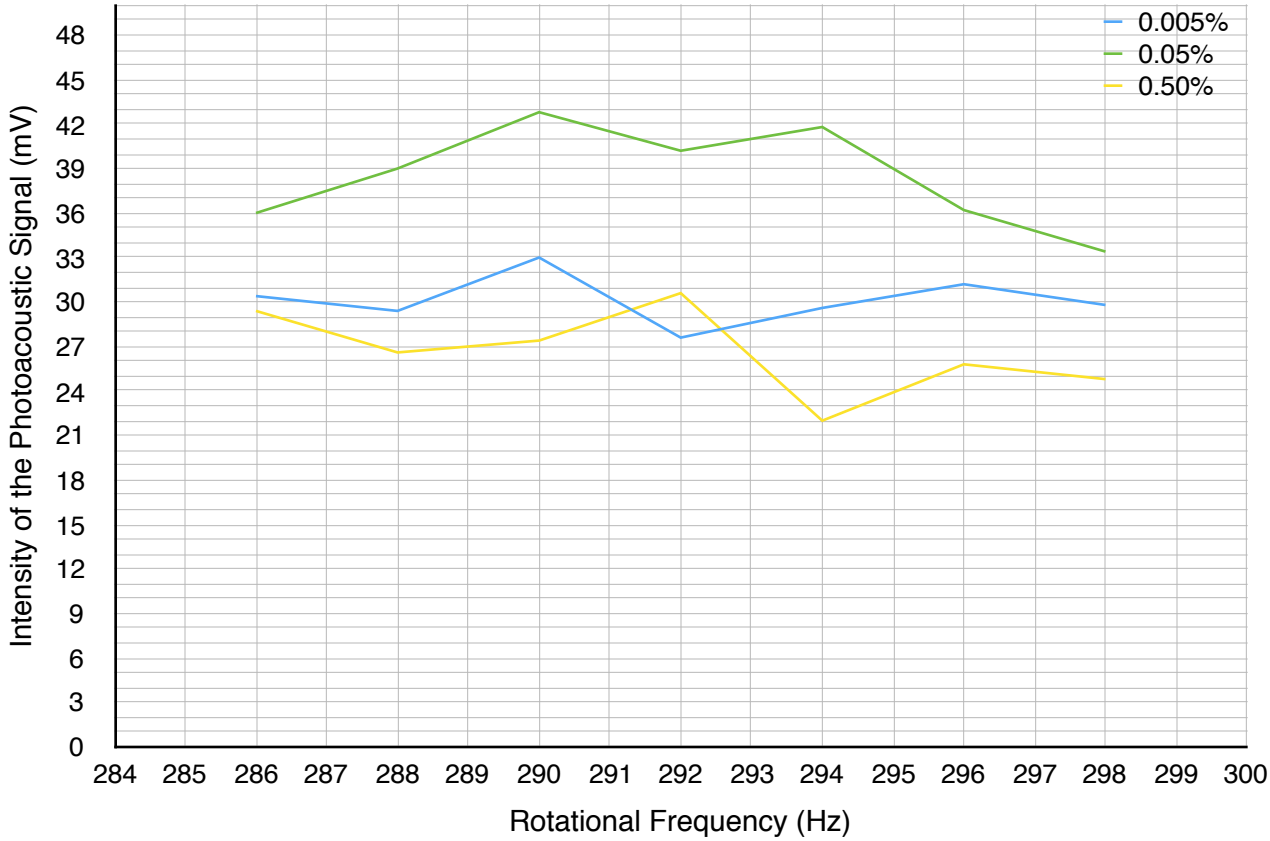

Figure XXVI. Superimposed spectra of 0.5%, 0.05%, and 0.005% concentration ethylene gas in Cell 1 by volume

The spectra generated when Cell 1 was filled with approximately 5%, 0.50%, and 0.05% ethylene gas by volume revealed a peak-like shape at a rotational frequency of 292 Hz. According to the data, ethylene gas was detected in Cell 1 when the concentration of ethylene gas was at least as low as 0.05% by volume or 500 ppm but not as low as 0.005% by volume or 50 ppm.

The four spectra generated for Cell 2 in this part of the research project were superimposed to help visualize how the intensity of the PA signal changed when the concentration of ethylene gas contained within Cell 2 was manipulated. Note that the internal radius of the cavity resonator was held constant. The resulting spectra can be found in Figures XXVII and XXVIII.

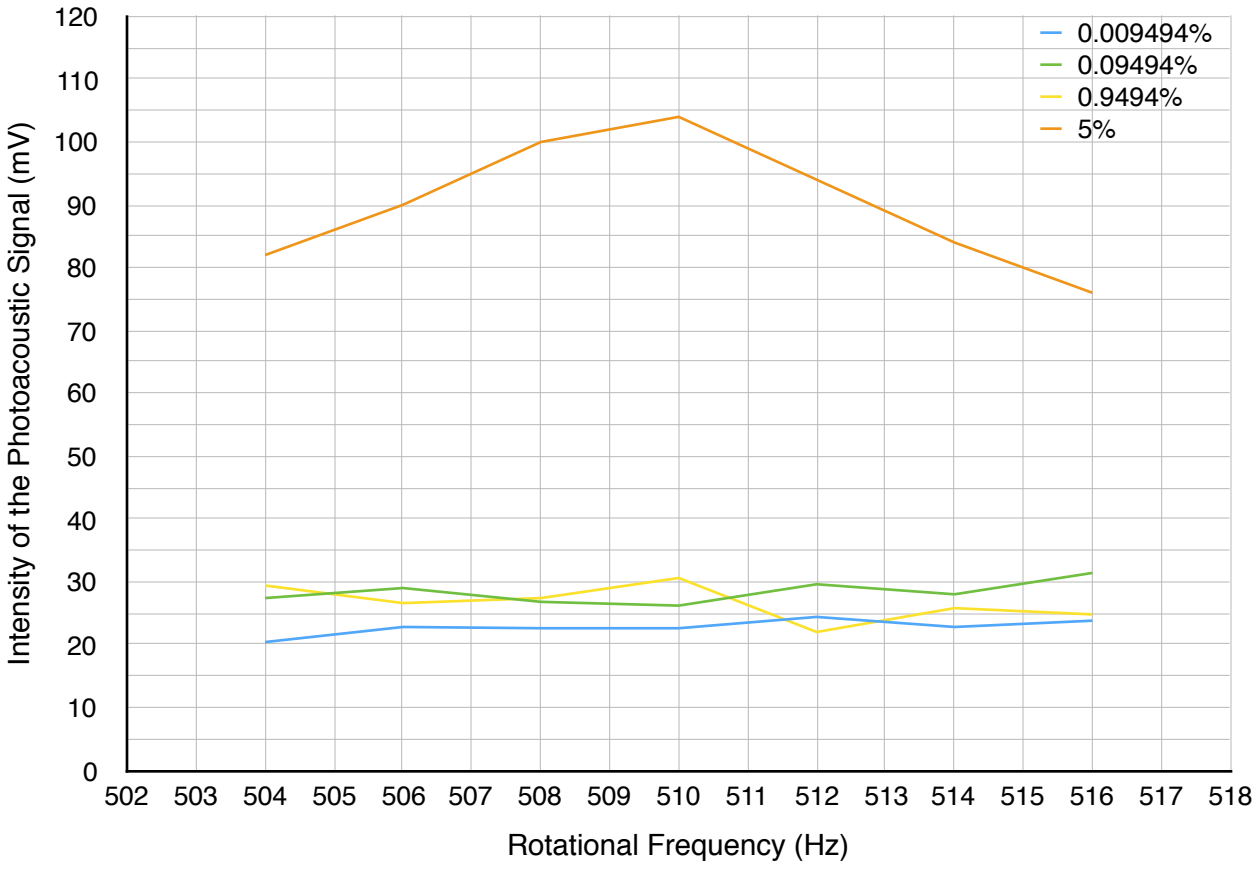

Figure XXVII. Superimposed spectra of 5%, 0.9494%, 0.09494%, and 0.009494% concentration ethylene gas in Cell 2 by volume

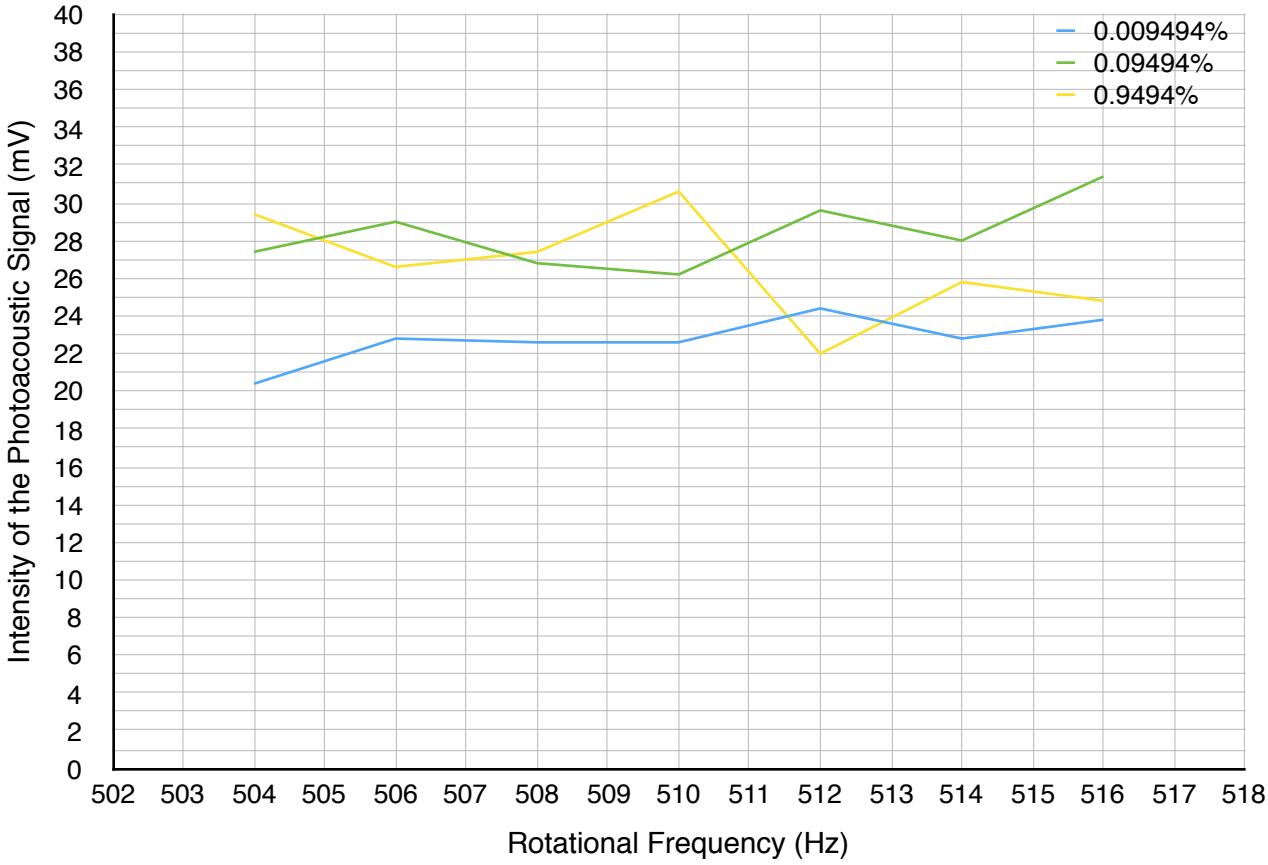

Figure XXVIII. Superimposed spectra of 0.9494%, 0.09494%, and 0.009494% concentration ethylene gas in Cell 2 by volume

The spectra generated when Cell 2 was filled with approximately 5% and 0.9494% ethylene gas by volume revealed a peak-like shape at a rotational frequency of 510 Hz. According to the data, ethylene gas was detected in Cell 2 when the concentration of ethylene gas was at least as low as 0.9494% by volume or 9494 ppm but not as low as 0.09494% by volume or 949.4 ppm.

The four spectra generated for Cell 3 in this part of the research project were superimposed to help visualize how the intensity of the PA signal changed when the concentration of ethylene gas contained within Cell 3 manipulated. Note that the internal radius of the cavity resonator was held constant. The resulting spectra can be found in Figure XXIX.

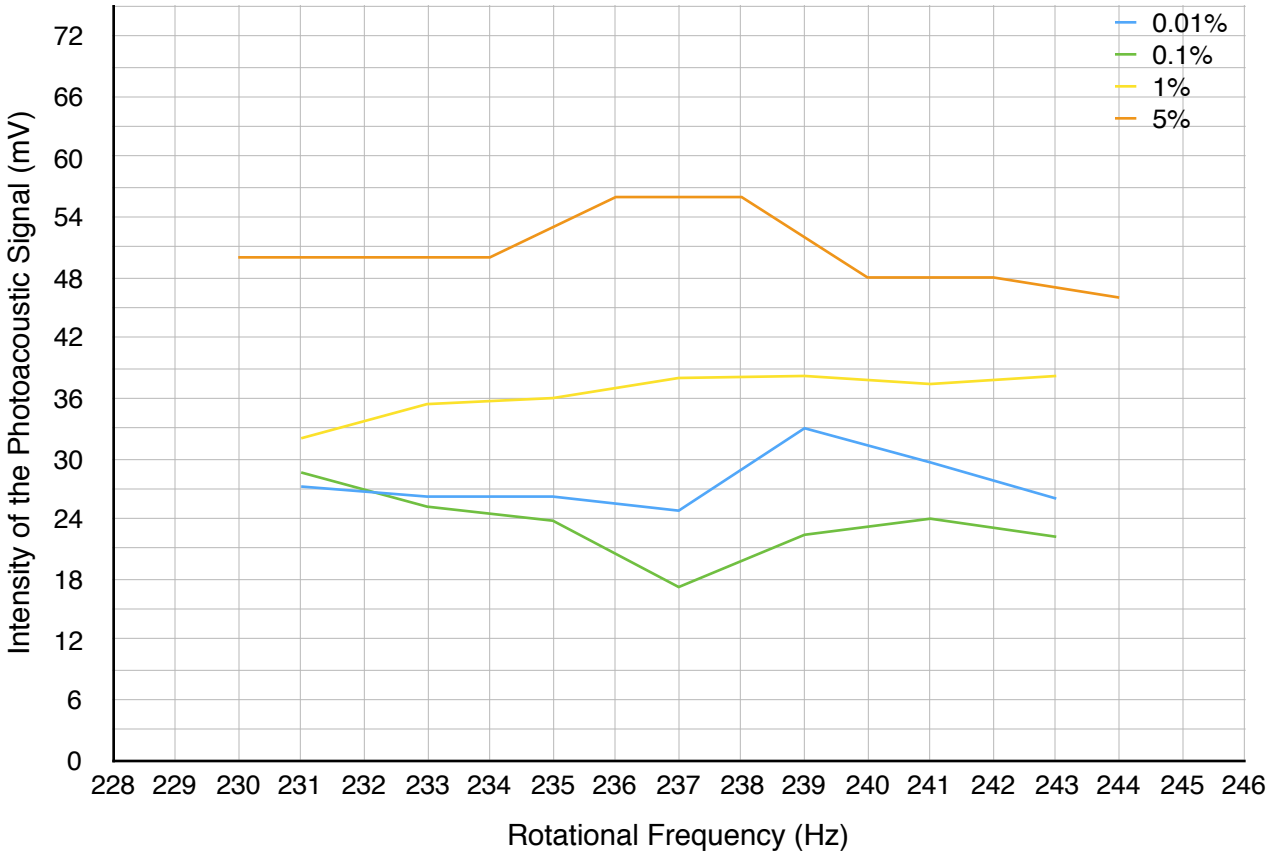

Figure XXIX. Superimposed spectra of 5%, 1%, 0.1%, and 0.01% concentration ethylene gas in Cell 3 by volume

The spectra generated when Cell 3 was filled with approximately 5% ethylene gas by volume revealed a peak-like shape at a rotational frequency of 237 Hz. According to the data, ethylene gas was detected in Cell 3 when the concentration of ethylene gas was at least as low as 5% by volume or 50,000 ppm but not as low as 1% by volume or 10,000 ppm.

Chapter 5: Discussion

Table of Contents

5.1: Infrared spectra of ethylene and nitrogen

This research project was performed to help contribute to the current understanding of the PA effect of ethylene gas. Various aspects of the experimental setup in this research project were independently manipulated to determine each of their effects on the PA signal produced by ethylene.

First and foremost, IR spectroscopy technique was utilized to verify that use of the buffer gas nitrogen would not interfere with detection and measurement of the analyte gas ethylene. The IR absorption spectra for both ethylene gas and nitrogen gas were obtained and can be found in

Figures VI and VII, respectively. According to Figure VI, the absorption wavelength of ethylene was experimentally verified to exist around the wavelength 10.6 μm. Furthermore, because ethylene was a strongly absorbing gas with a high absorption coefficient, the percent transmittance was 0% at 10.6 μm. According to Figure VI, the absorption spectra for nitrogen revealed no absorbance at or around 10.6 μm. This IR-inactive gas was, in fact, an appropriate buffer gas to use in this research project. These findings were consistent with the literature findings.

5.2: Experimental runs with manipulated parameters

In the second part of this research project, four aspects of the experimental setup were independently manipulated. These experimental parameters include the internal radius of the cavity resonator, power of the light source, concentration of analyte gas contained within the cavity resonator, and rotational frequency of the mechanical chopper. The spectra found in Chapter 4: Results, generated by superimposing the previously-obtained spectra for Runs A - O and Runs A2 - O2, were used to help visualize how manipulation of any of these four variables influenced the PA behavior of the analyte gas. Each spectrum used to create the superimposed spectra in Chapter 4: Results was individually evaluated to determine if any patterns were evident.

Upon initial evaluation of all spectra generated using the data sites for Runs A - O and A2 - O2, it was determined that in some cases but not all, as the rotational frequency of the mechanical chopper was increased, the intensities of the resulting PA resonance peaks (for spectra where more than two peak were observed) exponentially decreased. Literature references were used to support these findings. According to the journal article "Photoacoustic Spectroscopy for Process Analysis" and as previously mentioned in Chapter 2: Background, as the modulation frequency (and pulsation frequency) increases, the time in between each consecutive excitation and

de-excitation decreases, resulting in pressure fluctuations that are more difficult to distinguish among one another. Failure of the ICP transducer to detect and distinguish individual pressure fluctuations results in PA signals with relatively small intensities (17).

Additionally, upon initial evaluation of all spectra, it was determined that in some cases but not all, the PA resonance peaks (for spectra where more than two peaks were observed) were spaced out along the x-axis approximately equidistant from one another. According to the data, it was determined that PA resonance occurred at rotational frequencies with values that were multiples (approximately) of one another. For example, according to the data set for Run E, PA resonance occurred at rotational frequencies with values that were approximately 370 Hz apart. In other words, as the rotational frequency of the mechanical chopper was increased in 370 Hz increments beginning with 280 Hz, the frequency of the pressure fluctuations reflected off the boundaries of the cavity resonator at an arbitrary point in time was in phase with the natural frequency of the pressure fluctuations generated by the photon absorption of the analyte gas molecules at another arbitrary point in time. The presence or absence of the previously mentioned patterns—exponentially-decreasing intensities of the resonance peaks and evenly-spaced resonance peaks—were both used to help formulate a discussion about the quality of the PA effect. Experimental parameters that yielded both of the aforementioned patterns were determined to exhibit high quality PA behavior.

The spectra obtained using the data sets for Runs A - E and Runs A2 - E2 were superimposed to generate the spectra shown in Figures VIII and IX. These spectra were generated to help visualize how the intensity of the PA signal changed as the rotational frequency of the mechanical chopper and the concentration of analyte gas contained within Cell 1 were manipulated. The internal radius of the cavity resonator and the power of the light source were

held constant in both figures. Upon evaluation of the spectra found in Figure VIII, the spectra for Runs A - E were determined to possess both exponentially-decreasing intensities of the resonance peaks and evenly-spaced resonance peaks. As the concentration of analyte gas contained within Cell 1 was increased from 5% to 100%, the intensities of the resonance peaks also increased, and the resonance peaks were shifted to slightly lower rotational frequencies. A select range of rotational frequencies from Figure VIII was magnified to generate the spectra shown below in Figure XXX. This spectra was generated to better show how the intensities of the resonance peaks increased as the concentration of analyte gas contained within Cell 1 was increased.

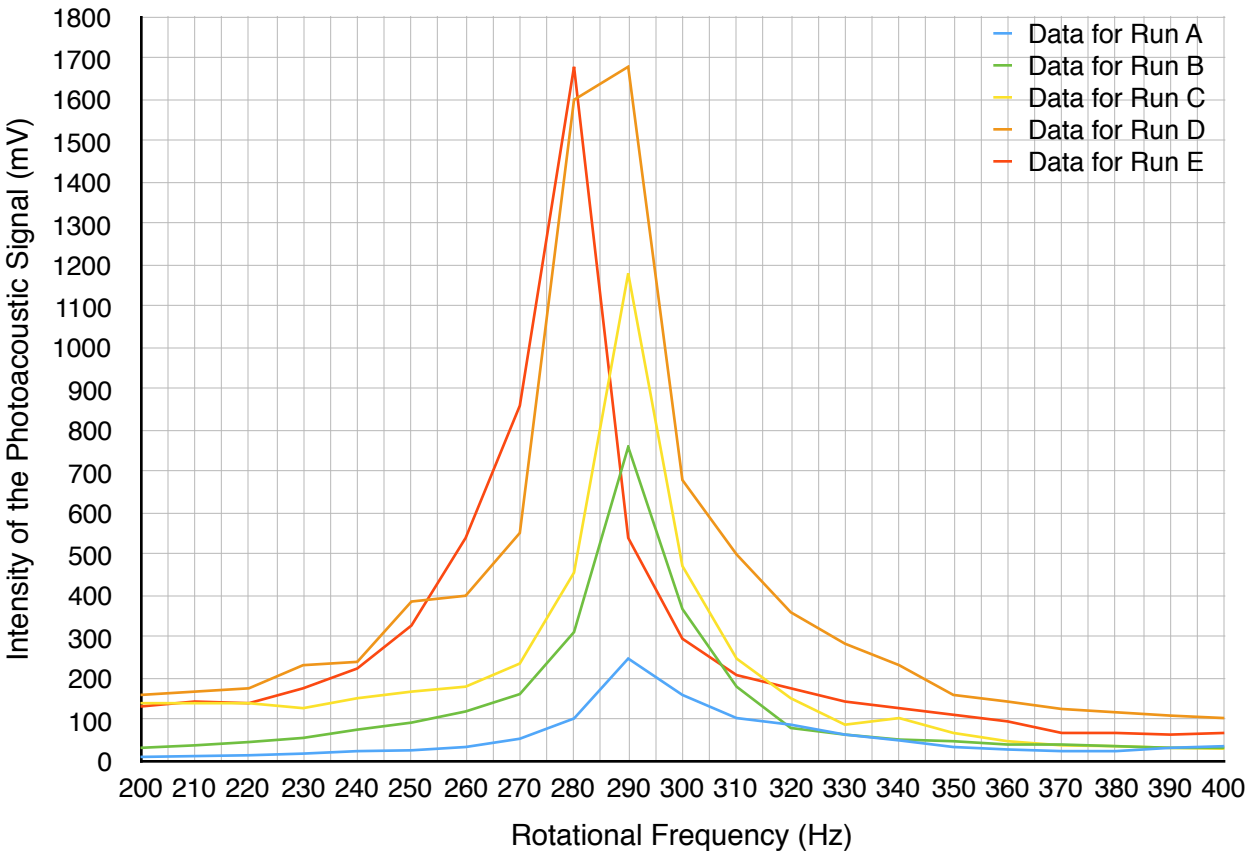

Figure XXX. Superimposed spectra for Runs A - E from 200 - 400 Hz

The Resonance Frequency Equation was used to justify the apparent shift to slightly-lower rotational frequencies as the concentration of the analyte gas was increased. According to Equation II, the resonance frequency, represented by the variable $f_{res,}$ is proportional to the square root of one (1) divided by the relative concentration of the gas solution contained within the cavity resonator, represented by the variable M, or the theoretical molecular mass for the analyte-buffer gas solution. This relationship is represented below in Equation IV.

$$Equation\ IV.\ f_{res} \propto \sqrt{\frac{1}{M}}$$

For Runs A2 - E2, the resonance frequencies were plotted as a function of the square root of one (1) divided by the relative concentration of the gas solution contained within the cavity resonator [determined by multiplying the molecular mass for each gas (28.0532 amu for ethylene and 28.01345 amu for nitrogen) by the relative abundances for each gas, then adding those products together]. The resulting graph can be found below in Figure XXXI, and the data used to generate this graph can be found below in Table IX. A line-of-best-fit was plotted through the data points. This line had a positive slope and a determination coefficient of 0.9837. These findings were consistent with Equation II.

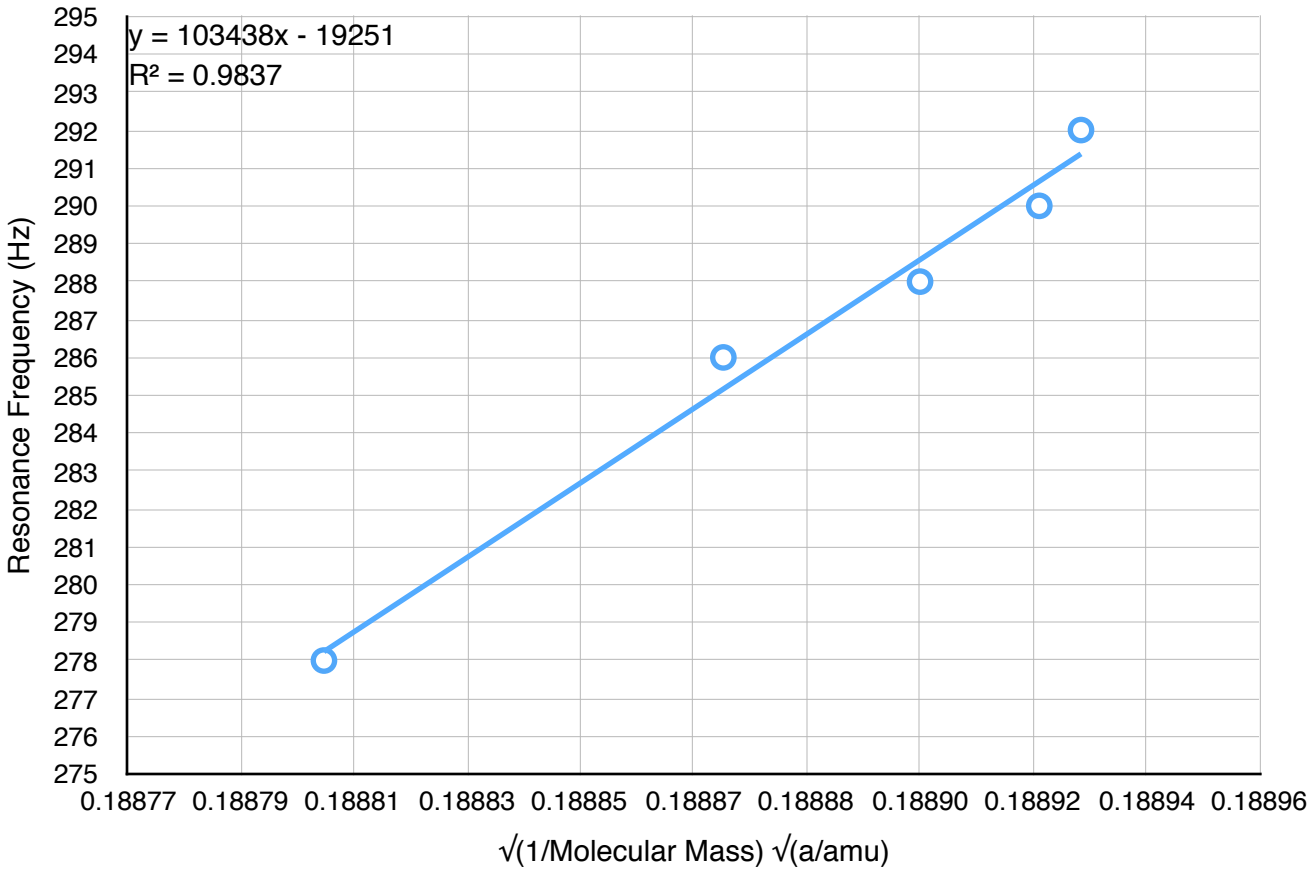

Figure XXXI. Resonance frequencies vs. square root of one (1) divided by relative concentration of the gas solution contained within the cavity resonator

Table IX. Data used to generate Figure XXXI

Run	Relative abundance of C_2H_4 (%)	C_2H_4 contribution towards theoretical molecular mass (amu)	Relative abundance of N_2 (%)	N_2 contribution towards theoretical molecular mass (amu)	$(1/\text{Molecular Mass})^{0.5}$ $(1/\text{amu})^{0.5}$
A	5	1.40267	95	26.6127	0.188930
B	10	2.80532	90	25.2121	0.188923
C	25	7.01330	75	21.0101	0.188903
D	50	14.0266	50	14.0067	0.188870
E	100	28.0532	0	0	0.188803

The individual data sets used to generate the individual spectra found in Figure XXX were normalized, so that the maximum values for the intensities of the resonance peaks were all equal to 1.0. These normalized data sets were used to generate the spectra shown below in Figure XXXII. This spectra was generated to better show how the intensities of the resonance peaks were shifted to slightly lower rotational frequencies as the concentration of analyte gas contained within Cell 1 was increased.

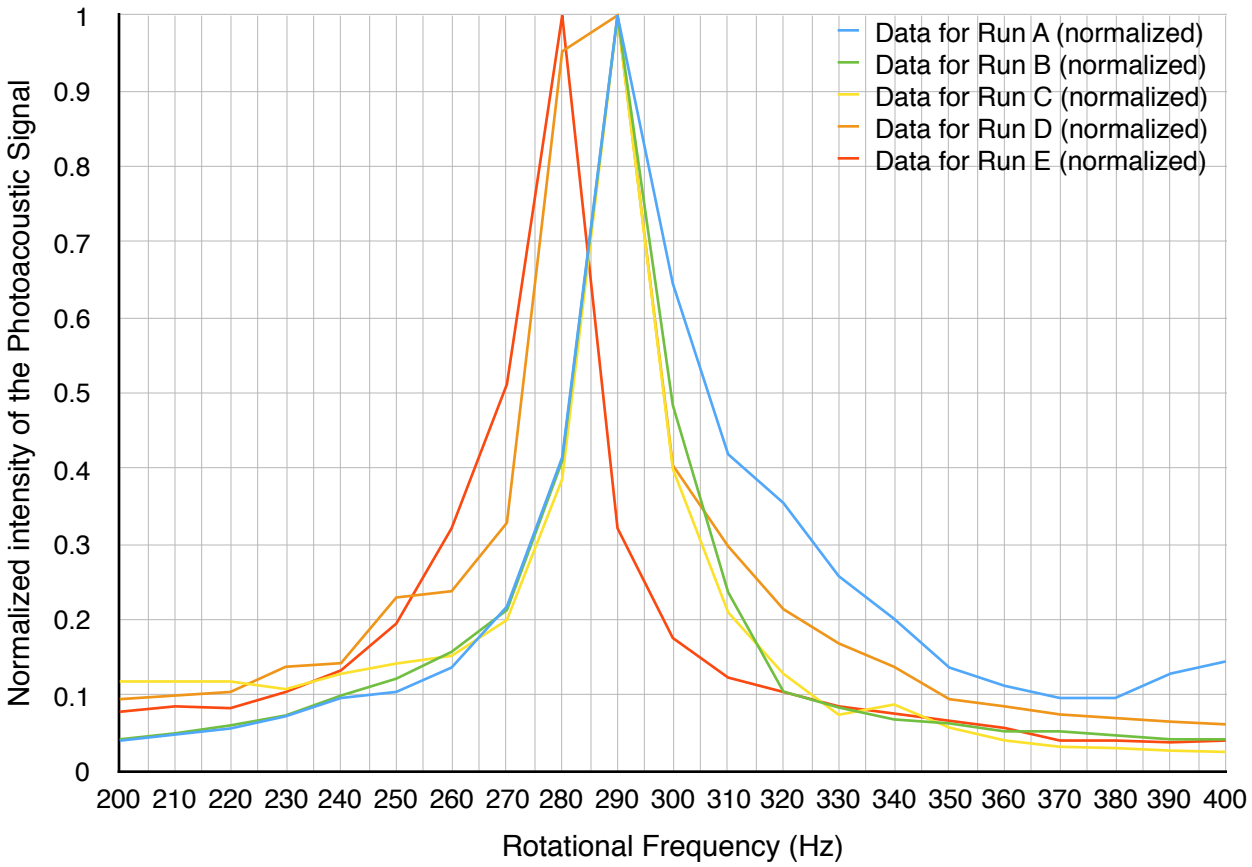

Figure XXXII. Normalized superimposed spectra for Runs A - E from 200 - 400 Hz

The spectra obtained using the data sets for Runs F - J, F2 - J2, K - O, and K2 - O2 were superimposed to generate the spectra shown in Figures X, XI, XII, and XIII, respectively. These spectra were generated to help visualize how the intensity of the PA signal changed as the rotational frequency of the mechanical chopper and the concentration of analyte gas contained within Cells 2 and 3 were manipulated. The internal radii of each cavity resonator and the power of the light source were held constant. Upon evaluation of the spectra found in Figure X, the spectra for Run F, H, and I were determined to possess both exponentially-decreasing intensities of the resonance peaks and evenly-spaced resonance peaks. The spectrum for Run G was determined to possess some exponentially-decreasing intensities of the resonance peaks and to possess evenly-spaced resonance peaks. The spectrum for Run J was determined to possess some exponentially-decreasing intensities of the resonance peaks and some evenly-spaced resonance peaks. The spectrum for Run K was determined to possess exponentially-decreasing intensities of the resonance peaks and to not possess evenly-spaced resonance peaks. The spectrum for Run L was determined to not possess exponentially-decreasing intensities of the resonance peaks and to possess evenly-spaced resonance peaks. The spectrum for Run M was determined to not possess exponentially-decreasing intensities of the resonance peaks and to possess some evenly-spaced resonance peaks. The spectrum for Run N was determined to not possess exponentially-decreasing intensities of the resonance peaks nor evenly-spaced resonance peaks. Finally, the spectrum for Run O was determined to possess some exponentially-decreasing intensities of the resonance peaks and to not possess evenly-spaced resonance peaks. Unlike Cell 1, according to the data, there was no obvious correlation between the concentrations of the analyte gas contained within Cells 2 and 3 and the intensities of the resonance peaks. Additionally, there were no obvious correlations

between the concentrations of the analyte gas and the rotational frequencies at which resonance peaks appeared when the internal radius of the cavity resonator was kept constant.

The spectra obtained using the data sets for Runs A, F, and J were superimposed to generate the spectra found in Figure XIV. The spectra obtained using the data sets obtained for Runs A2, F2, and J2 were superimposed to generate the spectra found in Figure XV. These spectra were generated to help visualize how the intensity of the PA signal changed as the rotational frequency of the mechanical chopper and the internal radius of the cavity resonator were manipulated but the concentration of analyte gas contained within the cavity resonator was held constant at 5%. As the internal radius of the cavity resonator was increased, the intensities of the resonance peaks appeared to decrease at all corresponding resonance frequencies. This same phenomenon was observed for the spectra found in Figures XVI - XXIII. As the internal radius of the cavity resonator is increased, the distance that a pressure fluctuation can travel before striking the boundaries of the cavity resonator increases. Pressure fluctuations that can travel greater distances before striking a boundary within a cylindrical cavity resonator will likely possess longer wavelengths and, thus, shorter frequencies. Pressure fluctuations with longer wavelengths will experience PA resonance at shorter resonance frequencies. These resonance frequencies may exist at rotational frequencies lower than the lowest rotational frequency permitted by the particular mechanical chopper used in this research project. According to this theory, cavity resonators with large internal radii may generate resonance peaks with similar characteristics as those generated by a relatively smaller internal radii; however, the resonance frequencies at which these resonance peaks occur will be shifted to low rotational frequencies that may not be attainable given a particular mechanical chopper and/or frequency modulator.

Lastly, Figure XXIV was generated to help visualize how manipulating the power of the light source effected the intensity of the PA signal generated upon photon absorption by the analyte gas. A line-of-best-fit was plotted through the data points. This line had a positive slope and a determination coefficient of 0.9846. Based off these findings, it was determined that when the concentration of the analyte gas contained within the cavity resonator was held constant, the intensity of the PA signal increased as the power of the light source increased due to the increased number of incident photons available for absorption by the analyte gas molecules. These findings were consistent with Equation I.

After observing all data gathered in the research laboratory and after considering any theory found in both physical and online references, it was determined that PA spectroscopy was a reliable technique to detect and measure the concentration of ethylene gas when the internal radius of the cavity resonator was small, the power of the light source was high, the concentration of ethylene gas was high, and the rotational frequency of the mechanical chopper was low.

5.3: Detection limit experiment

Lastly, a detection limit experiment was performed to formulate a qualitative discussion about how manipulating the internal radius of the cavity resonator influenced the concentration threshold at which a PA signal could be detected. Noise is of particular concern whenever using PA spectroscopy to detect and measure ultra-low concentrations of an analyte gas. The background signal generated upon interaction of the photons emitted from the light source and the windows enclosing the cavity resonator is often greater and more problematic than the noise signal (10). The detection limits for ethylene using Cells 1, 2, and 3 were determined to be at least as low as 500

ppm, 9494 ppm, and 50,000 ppm, respectively. Each of these detection limits were determined to be relatively high in comparison to other trace gas detection techniques.

As the internal radius of the cavity resonator was increased, the detection limit also increased. In the second part of this research project, it was determined that as the concentration of the analyte gas contained within the cavity resonator increased, intensity of the resulting resonance peaks increased. This phenomenon was somewhat evident for Cell 1 according to the spectra found in Figures XXVII and XXVIII. According to these two figures, higher concentrations of analyte gas yielded PA signals with relatively higher intensities except when the concentration of the analyte gas contained within the cavity resonator was 0.50%. At this trace concentration, the intensity of the resulting PA signal was lower than the intensities of the resulting PA signals when the concentrations of the analyte gas were 0.05% and 0.005%. This behavior is inconsistent with the PA behaviors observed in the second part of this research project. Because the intensity of the PA signal is proportional to the magnitude of the pressure fluctuations generated upon absorption of the incident photons by the analyte gas molecules, the intensity of the PA signal may have been lower-than-expected if the distance between the cavity resonator and the light source was greater when measuring the intensity of the PA signal when the concentration was 0.50% than when the measuring the intensity of the PA signal when the concentration was 5%, 0.05%, or 0.005%. This inconsistency in technique would have resulted in an increased likelihood of photon dispersion in the air and a lower-than-expected number of photons reaching the cavity resonator. Despite this inconsistency in data, it was determined that the detection limit of ethylene using PA spectroscopy was lowest when the internal radius of the cavity resonator was also at its lowest. This part of the research was designed to qualitative, versus quantitative; the actual detection limit of ethylene was not determined.

5.4: Sources of uncertainty and future research

During the time span that this research project was conducted, possible sources of experimental uncertainty became increasingly evident. Sources of experimental uncertainty include, but are not limited to, misalignment of the radiation emitted from the continuous-wave CO_2 laser with the cavity resonator's lengthwise axis of symmetry, inconsistent placement of the cavity resonator (with regard to the distance between the cavity resonator and the light source), and use of equipment not intentionally designed to be used for PA spectroscopic experiments.

An effort was made to align the radiation emitted from the light source with the cavity resonator's lengthwise axis of symmetry. This was done by using a detector card capable of sensing non-visible infrared radiation. The detector card was placed between the cavity resonator and the light source and on the opposite end of the cavity resonator to ensure that the cavity resonator was positioned in such a way that the radiation emitted from the light source was successfully reaching, propagating through, and exiting through the opposite end of the cavity resonator. At higher concentrations of the analyte gas, the detector card could not be used to track the propagation of the laser radiation through the cavity resonator due ethylene's strongly absorbing nature. In other words, the radiation from the light source could not be detected using the card because most, if not all, incident photons that did successfully enter the cavity resonator were immediately absorbed upon interaction with the analyte gas molecules. Poor alignment of the laser radiation with the cavity resonator's axis of symmetry may have resulted in inconsistencies in PA signal intensity caused by uneven dispersion of the pressure fluctuations and inconsistent interference of the incident and reflected pressure fluctuations. These poorly dispersed pressure fluctuations may have been more difficult to detect and separate using the microphone. It is suggested that in future PA spectroscopy research, the position of the cavity resonator should be fixed in such a way that all

experimental runs could be performed more confidently knowing that the radiation emitted from the light source was successfully reaching, propagating through, and exiting the cavity resonator along the cylindrical axis of symmetry where the analyte gas molecules had the greatest chance of generating pressure fluctuations evenly in all directions.

Throughout this research project, the distance between the cavity resonator and the light source was unintentionally varied from one experimental run to another. It was eventually determined that the percentage of the photons emitted from the light source that actually reached and were transmitted through the windows enclosing the cavity resonator decreased as the distance between the cavity resonator and the light source increased. This argument was driven by the understanding that particulate matter in the air can scatter photons away from the original pathway. The attenuation in laser power could have resulted in an overall decrease in the intensity of the PA signal (when the concentration of the analyte gas contained within the cavity resonator was held constant). It is suggested that in future PA spectroscopy research, the cavity resonator be positioned at a fixed distanced away from the light source for all experimental runs to minimize inconsistencies in data caused by a loss in radiation via scattering in the air. By keeping the distance between the cavity resonator and the light source constant, use of PA spectroscopy as a trace gas detection technique can be performed more confidently knowing that any changes in the intensity of the PA signal are the result of changes in the analyte gas concentration and not changes in laser power.

Lastly, it is believed that the greatest inconsistencies in data obtained in this research project were the result of using a poorly-constructed PA detector assembled using apparatuses not intentionally designed to be used for PA spectroscopy research. Factors contributing to the less-than-ideal setup include, but are not limited to, the lack of a new continuous-wave light source, the

lack of a more uniformly-shaped set of cylindrical cavity resonators, and the lack of system capable of producing vacuum-like or near-vacuum-like conditions within the cavity resonator. It was believed that repeat use of the particular light source and controller used in this research project for other experiments in the past may have negatively affected its ability to emit consistent and high-power radiation. Upon detailed analyses of the data obtained in this research project, it was determined that several of the inconsistencies observed may likely the result of using cylindrical cavity resonators that were not uniformly-shaped. For experiments involving the manipulation of the internal radii, any changes in PA signal intensity observed should primarily have been the result of variations in internal radii and not the result of variations in the overall shape of the cavity resonator, itself. In this research project, the three cavity resonators were constructed using apparatuses that were not specifically designed for PA spectroscopic experiments. The effect that the three cavity resonator's variation in shape had on the PA signal became increasingly evident for Cells 2 and 3. Lastly, it was also believed that inconsistencies in data obtained were the result of using a non-vacuum or non-near-vacuum-like apparatus. For each experimental run performed in this research project, the cavity resonator was thoroughly rinsed and filled with the inert buffer gas nitrogen. The cavity resonator was then filled with pre-determined volumes of ethylene gas to achieve specific concentrations of analyte gas contained within the cavity resonator. In theory, it is impossible for a closed system to contain any gas solution whose volume is effectively greater than the volume of the closed system, itself. In this research project, it was assumed that the cavity resonator used was not entirely enclosed and that leakage could occur if need be. In a vacuum system, the exact pressure within the cavity resonator could have been regulated. Rather than assuming that the total pressure within the cavity resonator was 1 atm, the exact total pressure could have been determined and used to further discuss the PA

behavior of ethylene. It is suggested that in future PA spectroscopy research, a new continuous-wave light source, more uniformly-cylindrical cavity resonators, and a system capable of producing vacuum-like or near-vaccuum-like conditions be used to help minimize inconsistencies in data caused by less-than-ideal PA detectors.

Statement of Results

This research project was performed to determine which experimental conditions best enabled precise and accurate measurements of ethylene using PA spectroscopy as a form of trace gas detection. It was determined that PA spectroscopy technique was most reliable when the internal radius of the cavity resonator was small, the power of the light source was high, the concentration of ethylene gas was high, and the rotational frequency of the mechanical chopper was low. These experimental conditions should be considered by manufacturers when devising highly-sensitive, low-cost, portable systems for the measurements of ethylene gas both inside and outside the laboratory.

Acknowledgements

Dr. Han J. Park, Ph.D., Thesis Director

Dr. Manuel F. Santiago, Ph.D., Department Examiner

Dr. Titus V. Albu, Ph.D., Department Examiner

Grote Fund, Department of Chemistry and Physics, UTC

Innovations in Honors Program, Honors College, UTC

Chapel Cowden, Health and Science Instruction Librarian, Library, UTC

References

1. McNaghten, E.D.; Parkes, A.M.; Griffiths, B.C.; Whitehouse, A.I.; Palanco, S. Detection of Trace Concentrations of Helium and Argon Gas in Mixtures by Laser-Induced Breakdown Spectroscopy [Online]. *Spectrochimica Acta.* **2009**, 1111-1118.
2. Harren, F. J. M.; Cotti, G.; Oomens, J.; Hekkert, S. L. Photoacoustic Spectroscopy in Trace Gas Monitoring. *Encyclopedia of Analytical Chemistry*; John Wiley & Sons: Chichester, 2012; pp. 2203-2226.
3. Gondal, M. A.; Dastageer, A.; Yamani, Z. H. Laser-Induced Photoacoustic Detection of Ozone at 266 nm Using Resonant Cells of Different Configuration [Online]. *J. Environ. Sci. Heal. A.* **2009**, *44*, 1457-1464.
4. Janssen, S.; Schmitt, K.; Blanke, M.; Bauersfeld, M. L.; Wöllenstein, J.; Lang, W.; Ethylene Detection in Fruit Supply Chains [Online]. *Philos. T. Roy. Soc. A.* **2014**, *372*, 1-21.
5. Lutrell, W. E. Ethylene [Online]. *J. Chem. Health Safety*. **2016**, *23*, 43-45.
6. Bleeker, A. Ethylene [Online]. *Curr. Biol.* **2011**, *11*, 952.
7. Ritenour, M. A.; Brecht, J. K. Ethylene Treatments for Ripening & Degreening, 2013.
8. *Ethylene*; MSDS No. 001022 [Online]; Airgas USA: Radnor, PA, Feb 6, 2004. https://terpconnect.umd.edu/~choi/MSDS/Airgas/ETHYLENE.pdf (accessed Mar 5, 2017).
9. Esler, M.B.; Griffith, D.W.T.; Wilson, S.R.; Steele, L.P. Precision Trace Gas Analysis by FT-IR Spectroscopy. 1. Simultaneous Analysis of CO_2, CH_4, N_2O, and CO in Air [Online]. Anal. Chem. **2000**, 72, 206-215.
10. Miklós, A.; Hess, P.; Modulated and Pulsed Photoacoustics in Trace Gas Analysis. Anal. Chem. **2000**, 72, 30-37.

11.Murphy, W. S.; Park, H. J. Detecting Photoacoustic Signals of Sulfur Hexafluoride at Varying Microphone Positions [Online]. *Open J. Phys. Chem*. **2016**, *6*, 49-53.

12.Park, H. J.; Murphy, W. S. A Study of the Photoacoustic Effect in SF_6 at High Concentrations and at Trace Detects in N_2 [Online]. *Journal of Undergraduate Chemistry Research*. **2015**, *14*, 90-92.

13.Park, H. J. Photoacoustic Effect and Sonoluminescence Generated by Laser Initiated Exothermic Chemical Reactions. Ph.D. Thesis, Brown University, Providence, RI, 2011.

14.Rosencwaig, A. Photoacoustic Spectroscopy of Solids [Online]. *Phys. Today* **1975**, *28*, 23-30.Miklós, A.; Hess, P. Application of Acoustic Resonators in Photoacoustic Trace Gas Analysis and Metrology [Online]. *Rev. Sci. Instrum*. **2001**, *72*, 1937-1955.

15.Ball, D. W. Photoacoustic Spectroscopy [Online]. *Spectroscopy* **2006**, *21*, 14-16.

16.Photoacoustic Spectroscopy, Theory. *Encyclopedia of Spectroscopy and Spectrometry;* Academic Press: San Diego, 1999; pp. 1815-1822.

17.Schmid, T. Photoacoustic Spectroscopy for Process Analysis [Online]. *Anal. Bioanal. Chem.* **2006**, *384*, 1071-1086.

18.*Nitrogen*; MSDS No. 00104 [Online]; Airgas USA: Radnor, PA, May 26, 2016. https://www.airgas.com/msds/001040.pdf (accessed Mar 5, 2017).

19.Kaneko, F.; Monjushiro, H.; Nishiyama, M.; Kasai, T. Photoacoustic Experimental System to Confirm Infrared Absorption Due to Greenhouse Gases [Online]. *J. Chem. Educ*. **2010**, *87*, 204-206.